

Templated ligation can create a hypercycle replication network

Shoichi Toyabe^{1, 2} and Dieter Braun¹

¹ Systems Biophysics, Physics Department, NanoSystems Initiative Munich and Center for Nanoscience, Ludwig-Maximilians-Universität München, Amalienstrasse 54, 80799 München, Germany

² Department of Applied Physics, Graduate School of Engineering, Tohoku University, Aramaki-aza Aoba 6-6-05, Aoba-ku, Sendai 980-8579, Japan

The stability of sequence replication was crucial for the emergence of molecular evolution and early life. Exponential replication with a first-order growth dynamics show inherent instabilities such as the error catastrophe and the dominance by the fastest replicators. This favors less structured and short sequences. The theoretical concept of hypercycles has been proposed to solve these problems. Their higher-order growth kinetics leads to frequency-dependent selection and stabilizes the replication of majority molecules. However, many implementations of hypercycles are unstable or require special sequences with catalytic activity. Here, we demonstrate the spontaneous emergence of higher-order cooperative replication from a network of simple ligation chain reactions (LCR). We performed long-term LCR experiments from a mixture of sequences under molecule degrading conditions with a ligase protein. At the chosen temperature cycling, a network of positive feedback loops arose from both the cooperative ligation of matching sequences and the emerging increase in sequence length. It generated higher-order replication with frequency-dependent selection. The experiments matched a complete simulation using experimentally determined ligation rates and the hypercycle mechanism was also confirmed by abstracted modeling. Since templated ligation is a most basic reaction of oligonucleotides, the described mechanism could have been implemented under microthermal convection on early Earth.

Our understanding of the emergence of life has made considerable progress in the last years, including advances in RNA catalyzed replication¹⁻⁸, synthesis of nucleotides⁹⁻¹⁰ and base-by-base replication with activated nucleotides^{11, 12}. Stable autocatalytic replications of sequence information are thought to be crucial for the evolution into more complex systems. Autocatalytic replications have been experimentally demonstrated with carefully designed ribozymes^{13, 14}, where an exponential growth of a group of mutually-catalytic ribozymes was observed. However, it remains difficult to imagine how complex autocatalytic system could have spontaneously emerged from a pool of random sequences.

However, first-order replication with an exponential amplification faces two inherent instabilities: the error catastrophe¹⁵ and a convergence to the fastest replicators¹⁶. First, most replication errors lead to inferior growth rates and fall behind the best replicating molecules. The balance between this selection and the error

rate shapes a group of sequences termed quasi-species which is localized in the sequence space. If the error rate exceeds a threshold, the selection can no longer suppress the accumulation of sequence errors and the quasi-specie vanishes. This is termed an error catastrophe. It is a major bottleneck for molecular evolution since primitive replicators will be highly erroneous. The dilemma is that strands need to be long and more structured to create catalytic activity to decrease the error rates, but the error threshold is much harder to reach for longer sequences. Therefore, even if a self-replicating molecule emerged at some point in a prebiotic soup of random sequences, this single molecule would struggle to sustain its sequence information against the sequence majority of the pool.

The second dilemma is that first-order exponential growth will inherently converge to the sequence combination with the highest replication rate, therefore suppressing the ability to use oligonucleotides for the storage of information. In many systems, the shortest sequences will dominate the population, famously shown by experiments of Spiegelman^{16, 17}. For templated ligation as mode of replication, the sequences with the highest thermodynamic binding stability would ligate fastest and dominate the sequence space, but would have no freedom to store genetic information. Both the error catastrophe and the convergence to a common sequence puts strong limits to the emergence of early molecular evolution.

The hypercycle proposed by Eigen is a theoretical concept to overcome both dilemmas¹⁵. A hypercycle is a cyclic network of replication cycles in which the product of a replication cycle catalyzes the reaction of a next replication cycle. This cooperative mechanism amplifies the sequence information at a higher order¹⁸. Let us consider a simple replication dynamics $\dot{x} = kx^{1+p} - dx = \alpha(x)x$ with $\alpha(x) = kx^p - d$. Here, k and d are the replication and the degradation rates which can differ between replicators. Unlike the ordinary exponential growth ($p = 0$), the hypercycle has a positive p , and its growth rate $\alpha(x)$ is enhanced with the accumulation of x . The frequency-dependent selection, or the Allee effect¹⁹, caused by this nonlinear growth stabilizes the wild types and raises the error threshold. Because by definition, mutants are less frequent than wild types, the mutants have a short lifetime. In addition, with the frequency-dependent selection, even the replicators with smaller k can survive and dominate if they once obtain a high frequency by fluctuations. Therefore, a more diverse pool of sequences will survive once they could gain a majority in one location. As a result, the system can explore more sequences and more diverse phenotypes, offering a wider search path for early molecular evolution.

Despite the above favorable properties of the hypercycle, the emergence of such a complex replication system with highly specialized cross catalysis was not expected from simple systems, at least in its original formulation. Although experiments have implemented designed replicator rings^{13, 14, 20, 21}, the systems are either driven by a combination of proteins or require special catalytic sequences. A cooperatively enhanced growth rate mechanism for general oligonucleotide sequences has not been demonstrated.

Here, we performed long-term replication experiments with a simple ligation chain reaction (LCR) of oligo DNA strands under molecule degradation conditions simulated by serial dilutions. We demonstrate that multiple LCR rings with overlapping templates show the replication properties of a hypercycle. The sequences form a cooperative meta ring of cross catalysis, grow at a higher order, and show the frequency-dependent selection of sequences. Furthermore, in simulations based on the experimentally determined ligation rates, we observed the spontaneous emergence of stable cooperative networks starting from a heterogeneous initial template concentrations over space. The mechanism could converge to a set of similar sequences at high concentration at a given location. It is important to understand that the mechanism does

not require the sequence to encode a catalytic function. Rather, it offers a passive self-selection before the onset of Darwinian evolution. Catalytic function however would obtain a significant head start at locations where the initial fluctuations and the cooperative amplification picked a functional sequence.

In a nutshell, the amplification mechanism works as follows (Figure 1). Ligation chain reactions form networks as they grow to larger strand lengths by templated ligation. We use the replication of oligonucleotides by the ligation chain reaction²² (supplement S1). Two typically shorter strands are first bound by a complementary template strand and then chemically connected. At elevated temperatures, the ligation is sensitive to many bases of sequence information in the vicinity of the ligation site. After linking, the product tends to be bound to the template, but it can dissociate at elevated temperature, which could for example be brought about in a periodic manner by thermal convection. Then, both strands act as new template and trigger two subsequent ligation reactions, resulting in exponential replication.

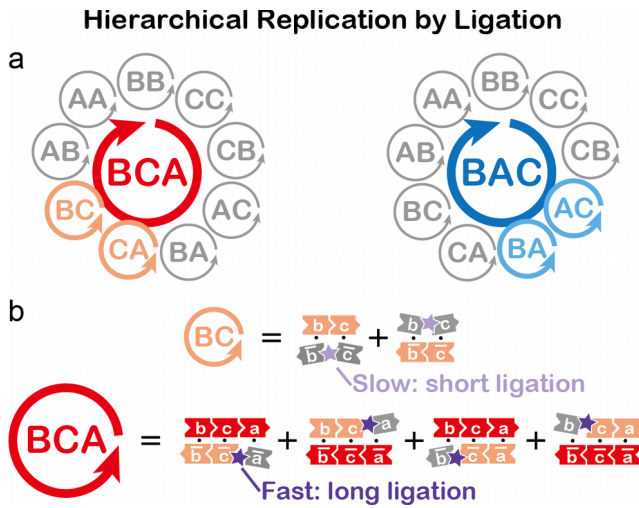


Figure 1: Multistability of replication by ligation. A ligation chain reaction replicates by connecting shorter strands on complementary sequences under thermal oscillations. Lowercase letters stand for 20 base long ssDNA sequences, capital letters denote both the sequence and its complement: $AB = \{ab, \bar{ba}\}$. At elevated temperatures, the higher stability of longer strands will lead to faster ligation. This creates a nonlinear cascade of cooperative replication reactions which show multistable dynamics. The replication becomes frequency dependent and sequences with higher initial concentrations are preferred.

To keep the system tractable, we work in our experiments with a reduced sequence space of three 20mer DNA sequences $a = 5'$ -atcag gtgga agtgc tgggt, $b = 5'$ -atgag ggaca aggca acagt and $c = 5'$ -attgg gtcac atcgg agtct and their reverse complement \bar{a} , \bar{b} , \bar{c} . We denote with capital letters both sequences $A = \{a, \bar{a}\}$, $B = \{b, \bar{b}\}$ and $C = \{c, \bar{c}\}$. We start the reaction with 40 mers, for example in Figure 3 with $BC = \{bc, \bar{cb}\}$ and $CA = \{ca, \bar{ac}\}$. The ligation is supplied with the substrates of short 20 mers A,B,C. The 40mers BC and CA initially will experience an exponential but slow growth, due to their short length and thus lower stability to bind to the 40mer template. The sequences BC and CA cooperate by binding at the sequence C and produce the novel 60 mer sequence BCA. Now the ligations $BC + A \rightarrow BCA$ and $B + CA \rightarrow BCA$ which due to their length show an enhanced ligation kinetics. These reactions show a positive feedback since also the ligation of BC and CA from A, B, C will be enhanced. Both leads to a non-linear, hypercycle replication characteristics. The system will decide between the replication of BCA or BAC depending on the initial sequence concentrations. As a result, majority sequence concentrations of the past are more stable against minority sequences and preserving the history of evolving systems.

Materials and Methods

Experiments. We performed ligation reactions of DNA strands with a thermostable Taq DNA Ligase (supplement S1). This protein catalyzed reaction is a laboratory proxy for a yet unknown prebiotic ligation reaction such as for example the synthetic *in situ* activation chemistry with EDC²³⁻²⁵. Substrate DNA strands are three complementary pairs $\{a, \bar{a}\}$, $\{b, \bar{b}\}$, and $\{c, \bar{c}\}$. The sequences were optimized to have similar ligation rates. We chose a ligation temperature of 67 °C where the 20 mer sequences bind less stable than 40mers and provide slower ligation as we will see (Figure 2a). The rationale for the high temperature is that prebiotic ligation would increase with temperature, yielding the fastest kinetics just below the melting temperature of the strands. To provide enough exchange between the strands, all experiments are performed under thermal cycling conditions (67 °C for 10 s and 95 °C for 5 s). This is a proxy for thermal microscale convection with a similar timescale^{17, 26}. In Figures 3 and 4, we performed serial dilutions to simulate the exponential molecular degradation.

Ligation reactions have the useful property to enhance the replicate length, as opposed to base-by-base replication which often suffer from Spiegelman's tyranny of the shortest^{16, 17}. To evaluate the sequence space of the system, we determined the concentration of binary sequence motifs $\langle AB \rangle$, $\langle AC \rangle$,... using a quantitative PCR method with low denaturation temperature (COLD PCR, supplement S2)²⁷ since deep sequencing would not have provided a comparable dynamic range of concentration between 0.1 pM and 100 nM.

Simulation. We used a brute force numerical approach to simulate the sequence network dynamics by creating systems of all sequence species with up to 2000 rate equations generated in C# and numerically solved using Mathematica (supplement S5) including the explicit serial dilutions. To be able to simulate the system, an effective thermodynamic binding approach was necessary. This assumes that the equilibration of the complex formation is faster than the thermal cycling and the binding of the ligase. A full temperature dependent simulation would be computationally too expensive. We thus used effective dissociation constants K_D and modeled the ligation rate k according to the experiments (Figure 2a, supplement S3). To obtain a full quantitative fit, 30 % changes in the ligation rate due to different ligase activity and a small degradation of the ligase had to be included in the simulations (supplement S5). The simulations are showed as solid lines in the graphs and reproduced the experimental results.

Results

Length selective ligation. We first probed the length dependence in linear, templated ligation (Figure 2). The 20-base sequence 'a' was ligated with Taq ligase to either **b** or **bc** on a 60-base template **cba**. Despite the thermal cycling, this replication was linear since the complementary substrate stock \bar{a} , \bar{b} , \bar{c} was missing. Analyzed by quantitative PCR, The rate of product formation for the long sequence was 215 pM per cycle for **abc**, about 40-fold higher than the 5 pM per cycle for creating the short sequence ab which under the temperature conditions had a lower probability to bind (Figure 2a). The experiments were used to quantify ligation for the subsequent simulations (supplement S3). We found effective dissociation constants $K_{D,20} = 193$ nM, $K_{D,40} = 4.5$ nM and $K_{D,60} = 2.7$ nM with 20, 40 and 60 denoting the overlapping nucleotide bases of hybridization and a ligation rate $k = 3.0$ nM⁻¹cycle⁻¹.

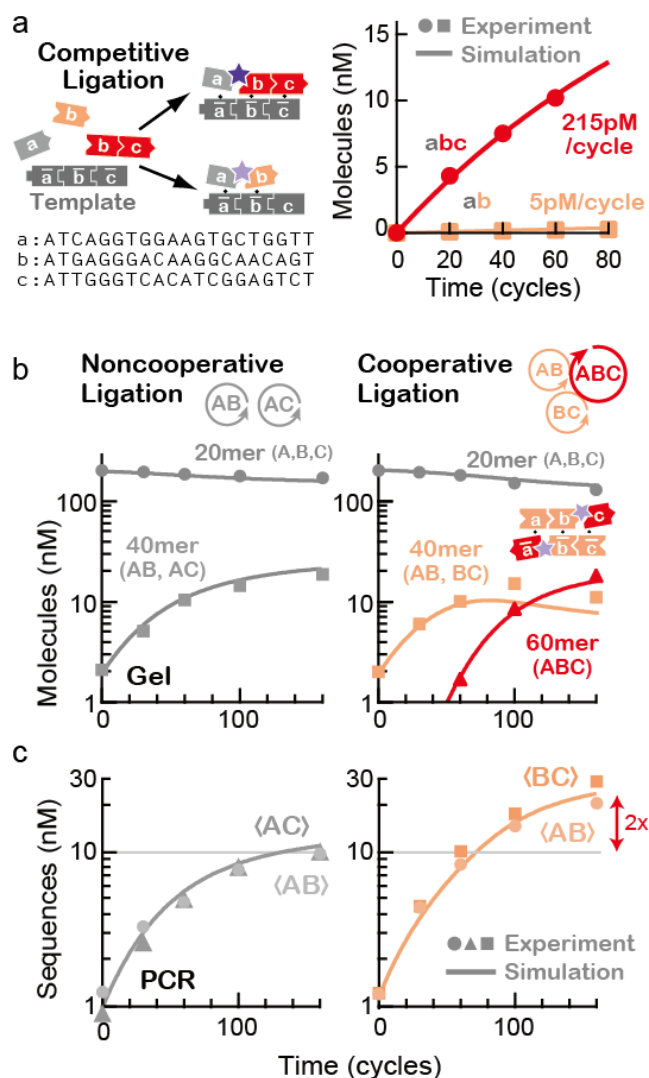


Figure 2: Enhanced replication by cooperative ligation. **a**, The ligation is 40-times faster on a 60 mer template \overline{cba} to connect the sequence 'a' with 'bc' than to link 'a' only with 'b'. **b**, The ligation dynamics of a non-cooperative sequence set AB and AC is compared with a cooperative set AB and BC. The latter can bind at the sequence B, creating the faster ligating 60 mer sequences ABC (inset). Both reactions are supplied with sequences A,B,C. The concentrations of the molecules was measured by gel electrophoresis. Solid lines are simulations (supplement S5) using the experimentally determined ligation rates in (a). **c**, The concentration of two-letter 40 mer sequence motifs $\langle AB \rangle$, $\langle AC \rangle$, and $\langle BC \rangle$ were quantified by a calibrated real time COLD PCR (supplement S2). For example, $\langle AB \rangle$ is given in this example by the concentrations of AB+ABC. The cooperation enhances the growth of 40 mer two-letter sequences about two-fold. This also increases the ligation of 40 mers from the supplied 20 mers. See Fig. S13 for the replicate experiment of (b) and (c).

Enhanced growth by cooperative replication. The ligation becomes autocatalytic once it is fed also by the complementary sequences \bar{a} , \bar{b} and \bar{c} ²². To probe the self-enhancing dynamics, we started the reaction with either a non-cooperative template pair (AB, AC) or a cooperative template pair (AB, BC). We probed the length distribution by gel electrophoresis (Figure 2b, supplement S4) and resolved the sequence dynamics by COLD PCR sequencing²⁷ (Figure 2c, supplement S2). The latter measures the concentrations of two-letter 40mer sequence motifs. With $\langle AB \rangle$ we denote all the concentration of the sequences containing AB. For example, the scheme adds the concentrations of molecules with the sequences ab , abc , $\bar{b}a$, or $\bar{c}b\bar{a}$.

When started with the non-cooperative pair AB and AC, an exponential growth of the sequence motifs <AB> and <AC> is found (Figure 2b and 2c, left). In contrast, with the cooperative pair AB and BC, we observed the growth of 60mer after sufficient replication of AB and BC sequences by the binding at the common B-sequence and concatenating to 60mer sequence ABC (Figure 2b, right). The longer sequence ABC works as an efficient template with the enhanced ligation rate for producing <AB> ($A + BC \rightarrow ABC$) and <BC> ($AB + C \rightarrow ABC$) as demonstrated in Figure 2a. This cooperative reaction implements a positive feedback: <AB> and <BC> grow more efficiently than the non-cooperative pair <AB> and <AC> in an about 2-fold increase (Figure 2c). The enhanced growth by cooperation is a central characteristic of hypercycles^{18, 28}.

Long term cooperative replication. To test how the replication evolves under continuous conditions, we supplied the 20mer substrates and the Taq ligase by serial dilution. Every 50 cycles, 1/6th of the solution was picked and transferred to a fresh solution containing 20mer DNA substrates and new DNA ligase. It also simulates an exponential long term degradation of the template sequence with a rate of 3.6 % per cycle which the replication has worked against to maintain the initial sequence information.

First, the non-cooperating pairs BA and BC were chosen (Figure 3a). Both withstood the exponential degradation, demonstrating their exponential replication, and settled into a steady state determined by the rates of replication and serial dilution. However, this mutual symmetry broke down when the motif CA was initially present (Figure 3b). The sequence pattern BA was suppressed and approached extinction, whereas BC survived together with CA. It has to be noted that the need for substrates is symmetric, all motifs compete with a second one for the substrates A, B or C. So what broke the symmetry in favor for BC sequences and against BA sequences? Again, three letter sequences emerged. The meta-sequence BCA assembled from BC and CA, helping both BC and CA in their replication (Figure 1), but offering no template for BA. The alternative system where initially AC is present (Figure 3) shows that this was not due to a thermodynamic bias of 20mer substrates or from an imbalance in ligation. The simulation based on the parameters found from Figure 2a confirmed the nonlinear selection and provided a quantitative description for the experiment (Figure 3a-c, solid lines). The length dependence of competitive ligation offers an enhanced replication of long consensus sequences and tips the balance towards the sequences which can collaborate with already existing motifs.

Kinetics of cooperation can overcome a thermodynamic bias. We introduced a sequence bias of ligation by enhancing the thermodynamic binding stability of A and B compared to that of C (Figure 3d). We started a simulation with the initial concentrations of BA, BC, and CA of Figure 3b and determined the concentration ratio of BC over BA (Figure 3d). The cooperativity of the ligation kinetics is varied by changing the ratio of $K_{D,20}$ for the ligation of 20-bases over $K_{D,40}$ for longer bases. For a vanishing length dependence of ligation with $K_{D,20} / K_{D,40} = 1$, BA dominates over BC due to the introduced thermodynamic bias of binding. Though, if $K_{D,20} / K_{D,40}$ approaches 10, the cooperativity of the common sequence inverts the situation. BC now dominates over BA due to its faster kinetics, a situation also expected from the experimental value of $K_{D,20} / K_{D,40} = 43$. The kinetically driven cooperativity of ligation is therefore capable to overcome a significant thermodynamic sequence bias, allowing the system to amplify sequence motifs which are binding with lower affinity if they are present at an initially higher concentration. This enhanced the diversity of the accessible sequence space for evolution.

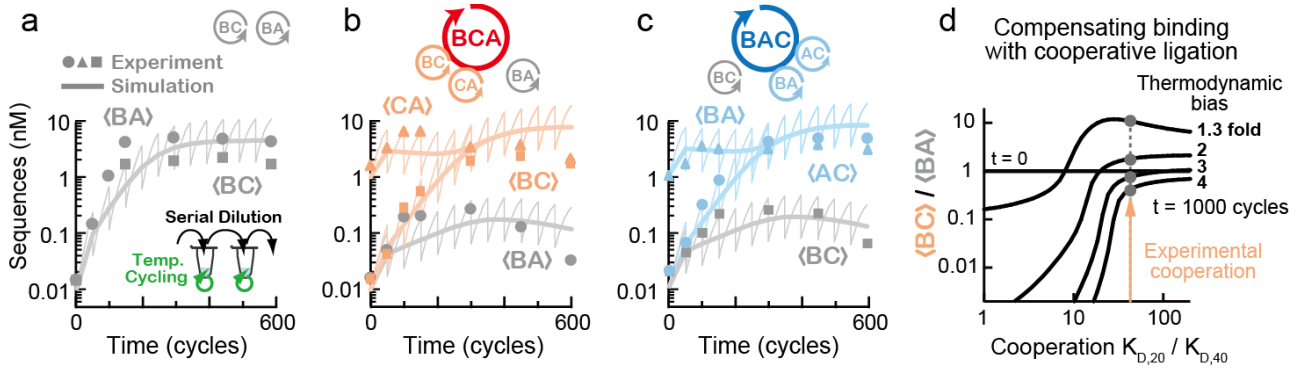


Figure 3: Selection of sequences by cooperation. Cooperative ligation replicates based on initial concentration and cooperating sequences. The reactions are performed under thermal cycling and serial dilution. The latter simulates molecule degradation and is used to replenish ligase and 20 mer educts. Solid lines simulations, also indicating the serial dilution dynamic. **a**, Initial 40 mer templates BA and BC replicate from 0.01 nM concentration to similar steady state concentrations, but cannot cooperate to form a 60 mer. **b**, The same reaction, now with an additional 1 nM of CA sequence. As the sequences CA and BC can cooperate by the 60 mer motif BCA, they both survive by replication while the non-cooperating sequence BA dies out. The initial concentration triggers a symmetry breaking by concentration-dependent sequence selection. **c**, When instead the AC sequence was initially added, the system picked BA instead of BC to create the sequence trimer BAC. **d**, We probed in simulation, how the kinetically driven cooperation can compensate a thermodynamic bias. The reaction in (b) was simulated with a thermodynamic bias where sequences A and B bind better than the sequence C. Without a cooperative mechanism ($K_{D,20} / K_{D,40} = 1$), the sequence BA dominate after 1000 cycles over BC, in contrast to the experimental finding. With the experimental value $K_{D,20} = 43 K_{D,40}$ the sequence BC dominates over BA. The cooperative kinetics can overcome an up to 3-fold thermodynamic bias. See Fig. S13 for the replicate experiment of (b) and (c).

Frequency dependent selection. In Figure 3, we have limited the length of the ligating sequences to 60 mer by not attaching phosphate groups at their ends. The same selection of majority sequences is found for fully ligating sequences which grow to considerable lengths (Figure 4). Here, we compared the replication of two competing groups of cooperating templates. On the one hand AB, BC, CA will support the common, periodic motif ...ABCABC..., but starting with CB, BA, AC sequences, the reverse motif ...CBACBA... should emerge. Both motifs are two out of 6 possibilities of the two-letter sequences to cooperate (supplement S6). Each of them is not promoting the ligation of the other two-letter sequences. As seen in Figure 4a, the sequences which initially have a majority concentration establish and survive in a steady state while the minority sequences decay exponentially (supplement S4). For both opposing biases, we observed splitting of the growth kinetics and confirmed that the initial bias was amplified, despite the fact that the replication at lower concentrations is faster due to reduced saturation effects. In contrast, an exponential replicator without interactions would immediately replicate both to the same high concentration levels (supplement S7). The length distribution was initially exponential, but after several cycles, long strands accumulated into fat tails. Similarly shaped distributions were predicted by ligation models²⁹⁻³¹. In our system, we find sequences with more than 160 bases, offering a good support for frequency-dependent selection of complex sequence. The simulations are predicting the selection dynamics.

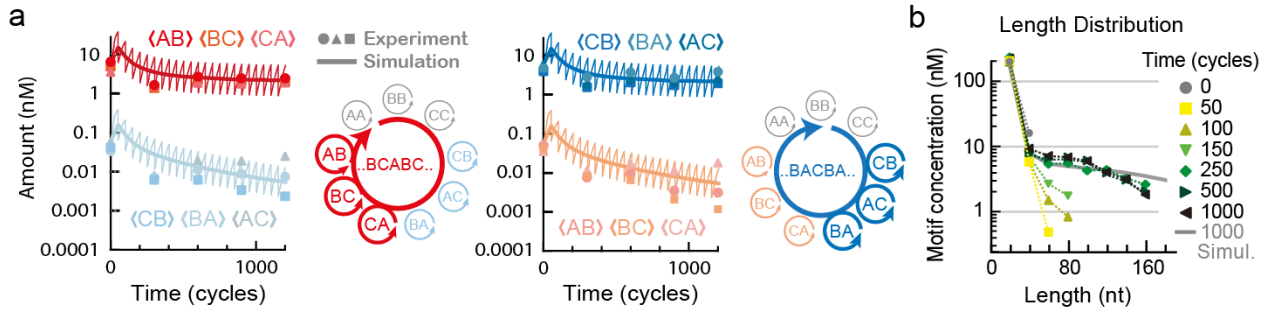


Figure 4: Frequency-dependent selection. Frequency dependent replication of two competing groups of cooperating sequence patterns. The group of three sequences AB,BC,CA generate “...BCABC...” while the sequences CB,BA,AC cooperate with the sequence “...BACBA...”. **a**, The reaction was started with a concentration bias of 6 nM vs. 60 pM for either AB,BC,CA, or CB,BA,AC. As before, the replication is fed with A,B,C sequences and subjected to simulated molecule degradation by serial dilution. In both cases, the majority patterns were sustained by replication against the serial dilution while the minority sequences died out. The simulation confirmed the experimental finding. See Fig. 13 for the replicate experiment. **b**, The cooperation generates long oligomers up to 160 bases from the initially 40 bases long starting sequences. The length distribution shows fat tails after 1000 cycles, both measured from gel electrophoresis in experiment (dots) and simulation (solid line).

Sequence patterns emerge despite diffusion from fluctuations in simulation. Because of the nonlinear selection described above, the state with uniform sequence concentrations is unstable. To extrapolate how the hierarchical replication dynamics could amplify small concentration fluctuations, we performed a long term simulation (Figure 5). Instead of assuming a well-mixed situation, we implemented diffusion along one dimension. The initial concentrations of all two-letter sequences (AA, AB, AC, BA, ...) were superimposed with 5% random concentration fluctuations. Despite diffusion, sequence patterns emerge which can be understood from the hierarchical replication structure. For example, AB, BC, CA cooperate towards sequences ...BCABCA... (Figure 5, red) or BC, CB, AA converge to ...BCBC... and ...AAAA... (Figure 5, yellow), selected from six possible sequence patterns (Figure S9). With a typical diffusion coefficient³² for DNA of $10^{-9} \text{ cm}^2/\text{s}$ and a temperature cycle of 30 s, the horizontal range would correspond to $\approx 5 \text{ mm}$. No patterns were found without cooperative rates of ligation ($K_{D,20}/K_{D,40} = 1$, Figure S8, supplement S7). Also systems under well-mixed conditions converged towards a stochastically chosen single cooperative network - all other sequence networks died out (supplement S6). This demonstrates that the nonlinear selection by the cooperative and hierarchical replication amplifies small fluctuations and spontaneously breaks the symmetry in the sequence space. It indicates that sequence individuality could be realized without any compartmentalization such as membranes.

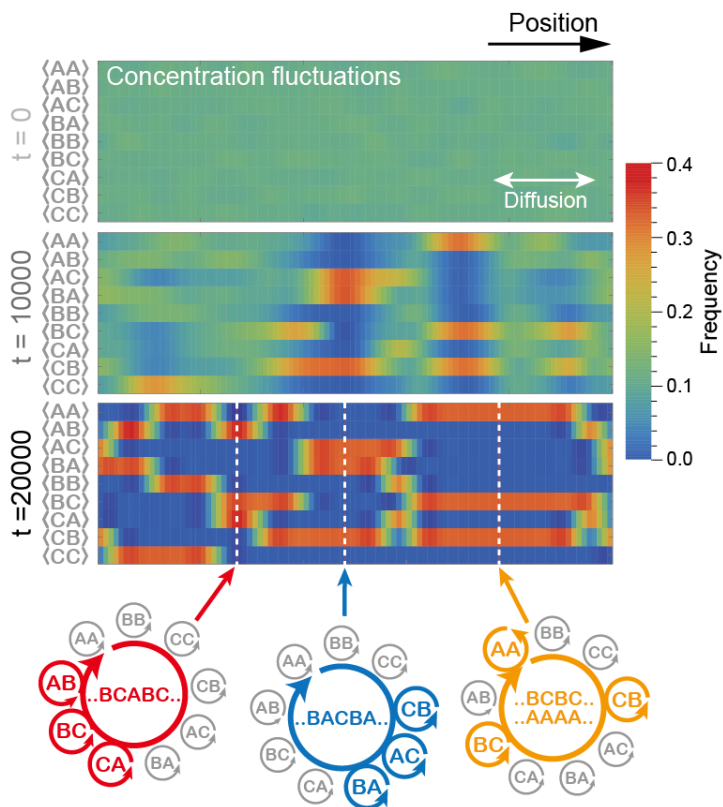


Figure 5: Cooperative replication creates patterns from fluctuations despite diffusion. The cooperative replication by ligation from two-letter motifs is simulated along one spatial dimension with molecule diffusion. The simulation starts with 5% concentration fluctuations of all 9 possible sequences. Cooperating sequences emerge as local patterns, demonstrating sequence multiplexing without compartmentalization.

Discussion

The experiments show that the sequence interaction under ligation can give rise to complex cooperative replication networks and show the two central properties of hypercycles, namely nonlinear growth and frequency-dependent selection^{15, 18, 28}. Sequences that cooperate in the ligation network replicate faster and can eventually dominate the sequence population. Not because they have an inherent, sequence dependent faster ligation rate^{33, 34}, but because they match with their longer sequences with the other ligation reactions in the sequence pool³⁵. This growth enhancement by sequence matching is seen in experiment for both the simplest binary cooperation (Figure 3b, c) and the trimeric cooperation networks (Figure 4a, b).

Due to the high order growth modes, the concentration becomes a major factor in replication. The experiments show how majority sequence networks can suppress minority sequence networks. Growth is therefore not only a function of the ligation rate, but the network of sequence cooperation can compensate a considerable thermodynamic binding bias (Figure 3d). As a result, sequences with lower ligation rate can survive and dominate by the cooperative growth rates, showing how a majority sequences can survive with a sub-optimal replication rates. This demonstrates how the sequence history of replication becomes important. It also increases the diversity of the sequence pool in early evolution.

This contrasts results from ordinary ligation with the first-order amplification^{13, 28}, in which only the fastest replicator wins. Since exponential first-order replication favors merely the sequences with the highest thermodynamic stability and ligation rate, it is likely that sequences composed of only G and C with low complexity would dominate the sequence space. But molecules with catalytic function require sophisticated high-order structures, which are unlikely for such thermodynamically stable and simple sequences. Here, frequency dependent selection from higher order growth opens new routes for the emergence of functional molecules.

Compared to base-by-base replicators, concatenation by ligation has an inherent tendency to produce sequences longer than the initial templates. Because longer sequences have more chances to cooperate with other sequences, longer strands are favored in cooperation networks. Indeed, we find a fat tail in the length distribution in our experiments (Fig. 4b). As a result, replication by ligation should be more prone to overcome the 'tyranny of the shortest' of base-by-base replicators, shown by Spiegelman¹⁶, where shorter strands dominate due to their faster replication rate.

The classical Hypercycles have been criticized to be sensitive to parasites that can take a free ride on the catalytic functions of the cycle³⁶. For cooperative ligation networks, in comparison, the catalytic role played by the template is symmetric. If there is a reaction where a strand X works a template to produce a strand Y, there is also a reversed reaction where Y works as the template to produce X. A simple mode of free riding is unlikely, and the network should be robust against parasites.

We measured the sequence dependence of the ligation rates and used it to model the experiments. The agreement with the experiments was very satisfactory. The only major parameters that needed slight adaptations were the overall ligation rate due to a different concentration of the ligation sites between experiments and a slightly varying degradation of the ligase depending on the protein batch used. This is why we can use the simulation to predict the system for scenarios too difficult to perform in experiment. The simulation (Fig. 5) and analytical theory (supplement S7) predicts that the cooperativity causes the instability of the uniform state and the amplification from small concentration perturbations into patterns of majority networks similar to quasi-species, even against diffusion. Unfortunately, the continuous feeding along one dimension, while demonstrated in the past with microfluidics³⁷, would be difficult to implement due to the predicted long experimental run times.

The cooperativity is caused by positive feedback and feed forward mechanisms. For example in Figure 2b, sequence matching 40mer two-letter sequences concatenate in a feed forward direction to form a 60mer with a three-letter sequence. The feedback loop is created backwards to the two-letter sequences since the created three-letter 60mers offer template sequences also to replicate more two-letter sequences. Both a sequence and concentration dependent replication metabolism emerges. The theoretical analysis suggests that the cooperation strength is measured by the kinetic enhancement $p = K_{D,20} / K_{D,40} - 1$. The nonlinear growth and selection are observed only for $p > 0$ (supplement S7). The value of p was determined to experimentally about 40 (supplement S3).

The shown mechanism bears strong similarity to chemical systems that amplify a chiral bias³⁸. We therefore expect it to be also able to purify backbone heterogeneity based on differential duplex stability³⁹. Mostly theoretical studies have been performed to analyze the length extension and expected reduction in sequence diversity in ligation²⁹⁻³¹. These studies also pointed out that ligation can lead to complex dynamics in sequence space. Especially, Tkachenko and Maslov pointed out how the length of overlap sequences is crucial for the increase in length under ligation²⁹. But no symmetry breaking and replication rate enhancing cooperativity was conjectured or experimentally demonstrated.

The ligation reaction is chemically simple. The details are not yet clear, but scenarios how it could be implemented prebiotically are explored and look promising^{10, 40-44}. In comparison, replication from single bases using ribozymes would be elegant, but requires a highly sophisticated machinery for the base-by-base replication^{7, 45}. Non-catalytic replication is a very interesting third possibility^{46, 47}, but similar to replication with ribozymes, a mechanism to implement hypercycle dynamics has not yet become clear in these systems.

Ligation provides a primitive replication function for sequences. As shown, the inherent cooperative characteristic of ligations can replicate complex sequence information stably. A problem however is that a polymerization mechanism is required to supply the ligation with the necessary short random oligonucleotides for ligation. Additionally, thermal cycling is required to eventually melt longer sequences. To implement both, a heat flow, for example across elongated rock pore systems on an early Earth^{32, 48}, could implement thermal cycling⁴⁹ and enhance the concentrations to aggregate oligonucleotides and enhance polymerization⁵⁰. Combined with a through flow, a thermal gradient can localize the replicated oligonucleotides and supply the replication reactions continuously. In a protein-catalyzed base-by-base replication, a thermal gradient was shown to overcome the dominance of short strands in and¹⁷.

Conclusion

Our experiments showed that a most basic mechanism - the joining of two DNA strands on a third template strand in a pool of diverse sequences - can form a cooperative cross-catalytic reaction network with higher-order replications of the sequence information. The higher-order growth dynamics can stabilize the replication of sequences against the inherent instabilities of simple first-order replicators and sets the stage for an enhanced Darwinian evolution under possible prebiotic conditions.

This work was supported by the Alexander von Humboldt Foundation, European Research Council (ERC) Starting Grant AutoEvo, the SFB 1032 Project A04, a grant from the Simons Foundation (SCOL 327125, DB), and JSPS KAKENHI (15H05460). We thank Jonathan Liu, Patrick Kudella and Alexandra Kühnlein for corrections on the manuscript.

Refere

1. Joyce GF, The antiquity of RNA-based evolution, *Nature* 418, 214-21 (2002)
2. Gilbert W, Origin of life: The RNA world, *Nature* 319, 618 (1986)
3. Bartel DP, Szostak JW, Isolation of new ribozymes from a large pool of random sequences, *Science* 261, 1411-8 (1993)
4. Attwater J, Wochner A, Holliger P, In-ice evolution of RNA polymerase ribozyme activity, *Nat. Chem.* 5, 1011-8 (2013)
5. Kruger K, Grabowski PJ, Zaug AJ, Sands J, Gottschling DE, Cech TR, Self-splicing RNA: autoexcision and autocyclization of the ribosomal RNA intervening sequence of *Tetrahymena*, *Cell* 31, 147-57 (1982)
6. Higgs PG, Lehman N, The RNA World: molecular cooperation at the origins of life, *Nat. Rev. Gen.* 16, 7 (2015)
7. Horning DP and Joyce GF, Amplification of RNA by an RNA polymerase ribozyme, *Proc. Nat. Acad. Sci. USA* 113, 9786 (2016)
8. Mutschler H, Wochner A, Holliger P, Freeze–thaw cycles as drivers of complex ribozyme assembly, *Nat. Chem.* 7, 502-508 (2015)
9. Powner MW, Gerland B, Sutherland JD, Synthesis of activated pyrimidine ribonucleotides in prebiotically plausible conditions, *Nature* 459, 239-42 (2009)
10. Bowler FR, Chan CK, Duffy CD, Gerland B, Islam S, Powner MW, Sutherland JD, Xu J, Prebiotically plausible oligoribonucleotide ligation facilitated by chemoselective acetylation, *Nat. Chem.* 5, 383-389 (2013)
11. Walton T and Szostak JW, A Highly Reactive Imidazolium-Bridged Dinucleotide Intermediate in Nonenzymatic RNA Primer Extension, *JACS* 138, 11996 (2016)
12. Deck C, Jauker M and Richert C, Efficient enzyme-free copying of all four nucleobases templated by immobilized RNA, *Nat. Chem.* 3, 603 (2011)
13. Lincoln TA, Joyce GF, Self-Sustained Replication of an RNA Enzyme, *Science* 323, 1229-32 (2009)
14. Vaidya N, Manapat ML, Chen IA, Xulvi-Brunet R., Hayden EJ, Lehman N., Spontaneous network formation among cooperative RNA replicators, *Nature* 72, 491 (2012)
15. Eigen M and Schuster P, The Hypercycle, *Naturwissenschaften* 65, 7-41 (1978)
16. Mills DR, Peterson RL, Spiegelman S, An extracellular Darwinian experiment with a self-duplicating nucleic acid molecule, *Proc. Nat. Acad. Sci. USA* 58, 217-24 (1967)
17. Kreysing M, Keil L, Lanzmich S, Braun D, Heat flux across an open pore enables the continuous replication and selection of oligonucleotides towards increasing length, *Nat. Chem.* 7, 203-8 (2015)
18. Szathmary E, Simple Growth Laws and Selection Consequences, *TREE* 6, 366 (1991)
19. Allee WC, *Animal Aggregations: A Study in General Sociology*, Univesity of Chicago Press, Chicago (1931)
20. Lee DH, Granja JR, Martinez JA, Severin K, Ghadiri MR, A self-replicating peptide, *Nature* 382, 525 (1996)

21. Ehricht R, Ellinger T, Mcaskill JS, Cooperative amplification of templates by cross-hybridization (CATCH), *FEBS J.* 243, 358-364 (1997)
22. Barany F, Genetic disease detection and DNA amplification using cloned thermostable ligase, *Proc. Nat. Acad. Sci. USA* 88, 189-93 (1991)
23. Taran O, Thoennessen O, Achilles K, von Kiedrowski G, Synthesis of information-carrying polymers of mixed sequences from double stranded short deoxynucleotides, *J. Sys. Chem.* 1, 9 (2010)
24. Griesser H, Tremmel P, Kervio E, Pfeffer C, Steiner UE, Richert C, Ribonucleotides and RNA Promote Peptide Chain Growth, *Angew. Chem. Int. Ed.* 56, 1219-1223 (2017)
25. Jauker M, Griesser H and Richert C, Copying of RNA Sequences without Pre-Activation, *Angew. Chem. Int. Ed.* 54, 14559-14563 (2015)
26. Mast CB, Braun D, Thermal Trap for DNA Replication, *Phys. Rev. Lett.* 104, 188102 (2010)
27. Li J, Wang L, Mamon H, Kulke MH, Berbeco R, Makrigiorgos GM, Replacing PCR with COLD-PCR enriches variant DNA sequences and redefines the sensitivity of genetic testing, *Nat. Med.* 14, 579-84 (2008)
28. Szathmary E, On the propagation of a conceptual error concerning hypercycles and cooperation, *J. Sys. Chem.* 4, 1 (2013)
29. Tkachenko, A. V., and Maslov, S., Spontaneous emergence of autocatalytic information-coding polymers, *J. Chem. Phys.* 143, 045102 (2015)
30. Derr J, Manapat ML, Rajamani S, Leu K, Xulvi-Brunet R, Joseph I, Nowak MA and Chen IA, Prebiotically plausible mechanisms increase compositional diversity of nucleic acid sequences, *Nuc. Acids Res.* 40, 4711 (2012)
31. Fernando C, Von Kiedrowski G, Szathmary E, A stochastic model of nonenzymatic nucleic acid replication: "elongators" sequester replicators, *J. Mol. Evol.* 64, 572-85 (2007)
32. Baaske P, Winert FM, Duhr S, Lemke KH, Russel MJ and Braun D, Extreme accumulation of nucleotides in simulated hydrothermal pore systems, *Proc. Nat. Acad. Sci. USA* 104, 9346 (2007)
33. Harada K, Orgel LE, Unexpected substrate specificity of T4 DNA Ligase revealed by in vitro selection, *Nuc. Acids Res.* 21, 2287-91 (1993)
34. Harada K, Orgel LE, In vitro selection of optimal DNA substrates for ligation by a water-soluble carbodiimide, *J. Mol. Evol.* 38, 558-60 (1994)
35. Worst EG, Zimmer P, Wollrab E, Kruse K, Ott A, Unbounded growth patterns of reproducing, competing polymers—, similarities to biological evolution, *New. J. Phys.* 18, 103003 (2016)
36. Bresch C., Niesert U, Harnasch D, Hypercycles, Parasites, and Packages, *J. Theor. Biol.* 85, 399-405 (1980)
37. McCaskill JS, Spatially resolved in vitro molecular ecology. *Biophysical chemistry*, 66, 145-158 (1997).
38. Soai K, Shibata T, Morioka H, Choji K, Asymmetric autocatalysis and amplification of enantiomeric excess of a chiral molecule, *Nature* 378, 767 (1995)
39. Gavette JV, Stoop M, Hud NV, Krishnamurthy R, RNA–DNA Chimeras in the Context of an RNA World Transition to an RNA/DNA World, *Angew. Chem. Int. Ed.* 55, 13204-9 (2016)
40. Mariani A, Sutherland JD, Non-Enzymatic RNA Backbone Proofreading through Energy-Dissipative Recycling, *Angew. Chem.* 129, 6663-6666 (2017)
41. Kramer M, Richert C, Enzyme-Free Ligation of 5'-Phosphorylated Oligodeoxynucleotides in a DNA Nanostructure, *Chem. Biodiv.* 14, e1700315 (2017)

42. Kalinowski M, Haug R, Said H, Piasecka S, Kramer M, Richert C, Phosphoramidate ligation of oligonucleotides in nanoscale structures. *ChemBioChem* 17, 1150-1155 (2016).
43. Patzke V, McCaskill JS, von Kiedrowski G, DNA with 3'-5'-Disulfide Links—Rapid Chemical Ligation through Isosteric Replacement, *Angew. Chem. Int. Ed.* 53, 4222-4226 (2014).
44. He C, Gállego I, Laughlin B, Grover MA, Hud NV, A viscous solvent enables information transfer from gene-length nucleic acids in a model prebiotic replication cycle, *Nat. Chem.* 9, 318-324 (2017)
45. Mutschler H, Wochner A, Holliger P, Freeze–thaw cycles as drivers of complex ribozyme assembly, *Nat. Chem.* 7, 502 (2015)
46. Engelhart AE, Adamala KP, Szostak JW, A simple physical mechanism enables homeostasis in primitive cells, *Nat. Chem.* 8, 448 (2016)
47. Walton T, Szostak JW, A kinetic model of nonenzymatic RNA polymerization by cytidine-5'-phosphoro-2-aminoimidazolid, *Biochem.* 56, 5739-5747 (2017)
48. Keil L, Hartmann M, Lanzmich S, and Braun D, Probing of molecular replication and accumulation in shallow heat gradients through numerical simulations, *PCCP* 18, 20153-9 (2016)
49. Braun D, Libchaber A, Trapping of DNA by Thermophoretic Depletion and Convection, *Phys. Rev. Lett.* 89, 188103 (2002)
50. Mast CB, Schink S, Gerland U, Braun D, Escalation of polymerization in a thermal gradient, *Proc. Nat. Acad. Sci. USA* 110, 8030-5 (2013)

Templated ligation can create a hypercycle replication network

Shoichi Toyabe^{1,2} and Dieter Braun¹

¹ Systems Biophysics, Physics Department, NanoSystems Initiative Munich and Center for Nanoscience, Ludwig-Maximilians-Universität München, Amalienstrasse 54, 80799 München, Germany;

² Department of Applied Physics, Graduate School of Engineering, Tohoku University, Aramaki-aza Aoba 6-6-05, Aoba-ku, Sendai 980-8579, Japan

S1. Ligation reactions

Single 20-base DNA strands serve as the minimum units. These oligomers are comprised of three complementary pairs (a , \bar{a}), (b , \bar{b}), and (c , \bar{c}) with one-base 5'-overhang, which reduces nonspecific ligations^{S1, S2}. The sequences are summarized in Table S1. 20-base and 40-base DNA oligomers of a PAGE (Polyacrylamide Gel Electrophoresis) or HPLC (High Performance Liquid Chromatography) purification grade were bought from Biomers (Ulm, Germany). Melting curves (Fig. S2) of the 20-mer strands were measured by using fluorescent dye specific to double strands, 1x SYBR Green I (ThermoFisher Scientific, MA, USA) and PCR cycler (Bio-rad, USA). The melting temperatures of the three monomeric unit pairs are all 67.5°C when the was 250 nM each.

The ligation reaction (Fig. S1) was performed with the typically 5 μ l reaction mixture containing 0.16 units/ μ l thermostable Taq DNA Ligase and 1x Taq DNA Ligase Buffer (New England Biolabs, MA, USA). The temperature cycling of 67 °C for 10 s and 95 °C for 5 s (Table S2) was generated by the real-time PCR cycler (Bio-rad, USA). The concentrations of the 20-base units were 200 nM in total (33.3 nM each).

Serial dilution was performed by a hand pipetting. Every 50 cycles, a small fraction of the solution was picked and transferred to a fresh solution containing substrates and DNA ligase. The dilution ratio was 1/6 every 50 cycles ($d = 0.036$ /cycle).

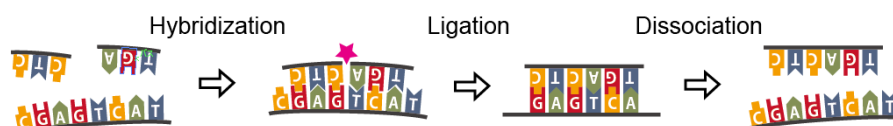


Figure S1: Ligation reaction. When two strands align next to each other on a third template strand by complementary hybridization, the strands are covalently connected at rate depending on the enzyme dynamics, but equally on the hybridization equilibrium of the strands. This reaction is much enhanced by ligase enzyme. The hybridization is stable when the temperature is lower than the melting temperature (T_m) between the two strands. T_m increases with the hybridization overlapping length. Therefore, the dissociation process is typically slow but can be enhanced by raising temperature. Temperature cycling makes molecules to oscillate between hybridized and dissociated states and enables them to rearrange, enabling for example sequential ligations and elongation of the oligomers by ligation. The process is exponential, as known from the simplest version of such a reaction, the ligase chain reaction^{S1}.

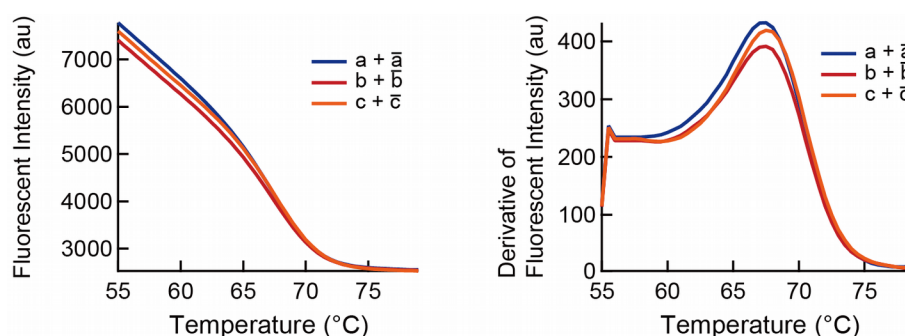


Figure S2: Melting curves of 20-base DNA strands serving as the monomeric units probed by 1x SYBR Green I, a fluorescent dye specific to double strands, performed in the Taq DNA ligase buffer. The peak positions of the derivative of fluorescent intensity correspond to the melting temperature (T_m). T_m of all the three complementary pairs were the same and 67.5 °C. The concentration of each mono unit was 250 nM.

	Sequences
A	a: 5' – ATCAGGTGGAAGTGCTGGTT – 3' \bar{a} : 3' – AGTCCACCTTCACGACCAAT – 5'
B	b: 5' – ATGAGGGACAAGGCAACAGT – 3' \bar{b} : 3' – ACTCCCTGTTCCGTTGTCAT – 5'
C	c: 5' – ATTGGGTCACATCGGAGTCT – 3' \bar{c} : 3' – AACCCAGTGTAGCCTCAGAT – 5'

Table S1: Sequences of 20-base DNA units comprised of three complementary pairs with one-base 5'-overhang.

Step		Temperature (°C)	Period (s)
1	Initial denaturing	95	20
2	Denaturing	95	5
3	Annealing and ligation	67	10
4	GOTO 2 (40 or 50 cycles)		
5	Heating	80	1
6	Rapid cooling	0	-
7	Serial dilution		
8	GOTO 1		

Table S2: Ligation reaction protocol. Temperature was cycled between 67 °C and 95 °C. After 40 or 50 temperature cycles, the sample was heated to 80°C, taken from the PCR cycler, cooled down on ice, and was transferred to a new fresh solution. This process prevents nonspecific ligations during the serial dilution. Ramps of the temperature changes are not included in the given times and are typically 3.3 deg/s for both the heating and cooling on the used Biorad CFX96 Real-Time PCR thermal cycler.

S2. Quantitative PCR (COLD PCR)

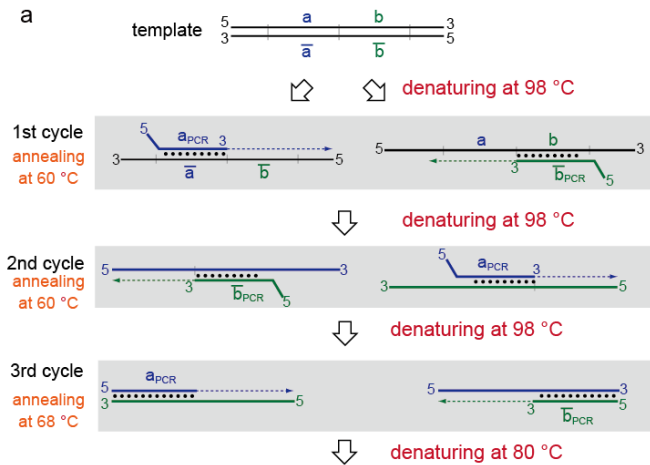
Sequence ordering was probed in terms of 40-base sequence motifs (Fig. 2a) by a modified real-time COLD PCR method for the data in Fig. 2a, 2c, 3a-c, and 4a^{S3}. In this method, only 40-base sequences (AB, AC, BA, BC, CA, CB) are amplified by using a low denaturing temperature (Fig. S3a and Table S3). PCR cycles are performed on a thermal cycler (BioRad, CFX96 Touch™ Real-Time PCR, USA) with a reaction volume of 2.4 μ l containing 0.02 units/ μ l Hotstart Phusion Polymerase (New England Biolabs, MA, USA), 1x detergent-free HF Phusion buffer (New England Biolabs), 200 μ M total dNTP mixture (New England Biolabs), 1x EvaGreen (Biotium, CA, USA), and 125 nM each of forward and reverse primers. The Phusion polymerase has no 5' \rightarrow 3' exonuclease activity. PCR solution was prepared on 96-well plates by a pipetting robot on the basis of ultrasonic liquid handling (LabCyto, USA).

The forward-primer sequences are a_{PCR} : GCCAT AAAGG TGGAA GTGCT GGTT, b_{PCR} : GCCAT AAAGG GACAA GGCAA CAGT, and c_{PCR} : GCCAT AAGGG TCACA TCGGA GTCT. The reverse-primer sequences are \bar{a}_{PCR} : GCGTA TTCCA GCACT TCCAC CTGA, \bar{b}_{PCR} : GCGTA TTTGT TGCCT TGTCC CTCA, and \bar{c}_{PCR} : GCGTA TTAAT CCGAT GTGAC CCAA. These sequences are similar to the corresponding ligation mono units but their 5'-end sequences are modified. Three bases at the 5' end were removed and short sequences GCCATAA (for forward primers) or GCGTATT (for reverse primers) were attached. These 5' short sequences are not complementary to the ligation products and increase the specificity of PCR amplification. We used primer pairs a_{PCR} and \bar{b}_{PCR} for probing AB, and b_{PCR} and \bar{c}_{PCR} for probing BC, for example.

In Fig. 1b and S5, we used a special longer substrate $bq = \text{ATGAG GGACA AGGCA ACAGT GAACT CAGTG TAGCC TCAGAT}$ for b in the ligations in order to differentiate ab and abc by PCR. We used higher denaturing temperature (98°C) for all the cycles with the primers a_{PCR} and $q_{PCR} = \text{GCGTA TTTGA GGCTA CACTG AGTTC}$ for detecting BC or a_{PCR} and \bar{c}_{PCR} , for detecting ABC.

We measured the amounts of the 40-base motifs by locating the horizontal positions of the real time PCR curves, C_t , by maxRatio method^{S4}. See Fig. S3b for the PCR curves and S3c and S3d for the estimated C_t values for calibration, where the real time PCR cycles were initiated by controlled template concentrations. We fitted these C_t -value series by logarithmic curves $[\text{Template}] = 2^{-\alpha(C_t - \beta)}$ and obtained the calibration parameters α and β (Table S4).

COLD PCR



Calibration

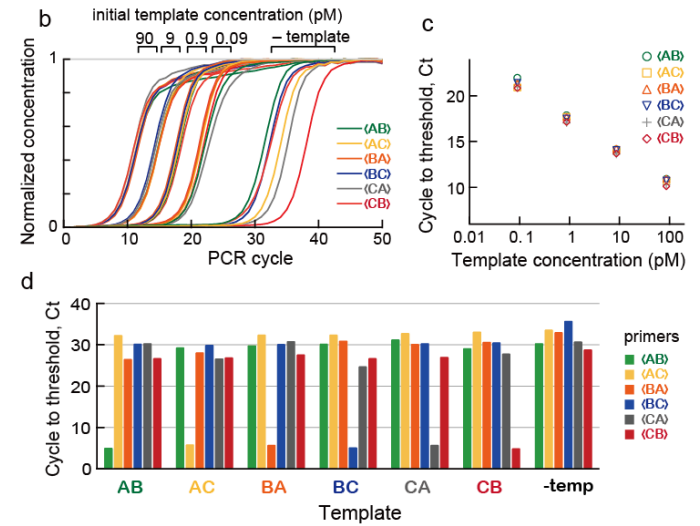


Figure S3: COLD PCR. a, By denaturing at a low temperature, only short strands of dimeric sequence motifs are amplified, confirmed by a melting curve analysis after the amplification. In the first three cycles, the denaturing temperature is high for denaturing ligation products, which possibly contain long double strands. b, Calibration curves of COLD PCR. a, We initiated the COLD PCR cycles by dimeric strands mixture containing AB, AC, BA, BC, CA, and CB or without templates of different concentrations. PCR cycles were performed with different primers. c, We analyzed the horizontal positions of the PCR curves, or the cycle to threshold denoted by C_t , by locating the cycling number where the ratio of the concentrations between two successive cycles becomes maximum^{S2}. Let x_n be the strand concentration at the n -th cycle. C_t is n that maximizes x_n / x_{n-1} . By fitting logarithmic curves to the C_t -value series, we obtained calibration parameters (Table S4). d, Nonspecific amplification was checked by measuring the C_t values of the COLD PCR cycles initiated by different dimeric template (1 nM) and amplified different primer sets. See Table S3 for the protocol of COLD PCR.

Step		Temperature (°C)	Period (s)
1	Initial denaturing	98	60
2	Denaturing	98	5
3	Annealing	60	15
4	Elongation and measurement	72	5
5	GOTO 2 (2 cycles)		
6	Cold denaturing	80	15
7	Annealing	68	15
8	Elongation and measurement	72	5
9	GOTO 6 (50 cycles)		

Table S3: COLD PCR protocol. Only in the nonspecificity test (Fig. S3d), the annealing temperature at the step 7 was changed to 67 °C, but this small difference had only a small effect on the cycles to threshold values of PCR amplifications.

Sequence motif	AB	AC	BA	BC	CA	CB
α	0.90	0.98	0.96	0.94	0.94	0.93
β	17.8	17.3	17.6	17.5	17.0	17.0

Table S4: Calibration parameters of COLD PCR, C_t values, obtained by fitting curves $[\text{Template}] = 2^{-\alpha(C_t - \beta)}$ (in the unit of nM) to the C_t values in Fig. S3b.

S3. Dissociation constant and ligation rate

In order to know the dissociation constants K_D and the ligation rate k (Fig. S4), we performed temperature cycling of ligation reactions without serial dilution (Fig. S5). The initial solution contains, for example, a , b and \overline{cba} (Fig. S5a). The substrates a and b are ligated on the template \overline{cba} and a product ab is produced. The ab strand does not template other reactions because the solution does not contain \overline{a} and \overline{b} . The amount of template strands does not increase and therefore the product grows only in a linear manner. By comparing the ligations $a + b \rightarrow ab$ and $a + bc \rightarrow abc$ on the template \overline{cba} , we obtain K_D and k as follows.

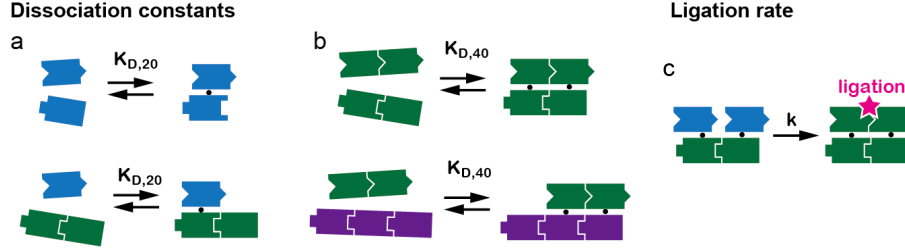


Figure S4: Dissociation constant K_D and ligation rate k . **a**, **b**, $K_{D,20}$ and $K_{D,40}$ are the dissociation constants of hybridization with the hybridization length one or two, respectively. The larger K_D is, the less stable strands hybridize. **c**, The ligation rate k is defined as the reaction rate that two strands aligned on a template are ligated.

We performed ligations on a template \overline{cba} and measured the time courses of the ligation products in the presence of the following three substrate sets by quantitative PCR, (i) $a + b$, (ii) $a + bc$, and competitive situation (iii) $a + b + bc$. The time courses were fitted by general saturation curves $y(t) = (v_0 / q) [1 - \exp(-qt)]$ with fitting parameters v_0 and q . The parameter v_0 is the growth rate at $t = 0$ and provides the information about K_D and k . We denote v_{ab} , v_{abc} , u_{ab} , and u_{ab} as the growth rates of $[ab]$ in (i), $[abc]$ in (ii), $[ab]$ in (iii), and $[abc]$ in (iii) respectively at $t = 0$. These growth rates provide the information about K_D and k .

For this simple ligation reaction, we could assume a comparably simple model of ligation and hybridization. For example, in the case of (i), the growth rate of the product ab becomes

$$\frac{d[ab]_0}{dt} = k_{ab} \frac{[a]_f [b]_f [\overline{cba}]_f}{K_{D,20} K_{D,20}}.$$

Here, $[]_f$ and $[]_0$ denotes the amount of free strands apart from the templates and the total amount of the strands, respectively. The conservation laws are

$$\begin{aligned} [a]_0 &= [a]_f + \frac{[a]_f [\overline{cba}]_f}{K_{D,20}} + \frac{[a]_f [b]_f [\overline{cba}]_f}{K_{D,20} K_{D,20}}, \\ [b]_0 &= [b]_f + \frac{[b]_f [\overline{cba}]_f}{K_{D,20}} + \frac{[a]_f [b]_f [\overline{cba}]_f}{K_{D,20} K_{D,20}}, \quad \text{and} \\ [\overline{cba}]_0 &= [\overline{cba}]_f + \frac{[a]_f [b]_f [\overline{cba}]_f}{K_{D,1} K_{D,20}} + \frac{[a]_f [\overline{cba}]_f}{K_{D,20}} + \frac{[b]_f [\overline{cba}]_f}{K_{D,20}} + \frac{[ab]_f [\overline{cba}]_f}{K_{D,40}}. \end{aligned}$$

By solving these equations at $t = 0$, we obtain the following equations

$$K_{D,20} = \alpha K_{D,40} \quad \text{and} \quad K_{D,40} = \frac{\beta - 1}{\alpha - \beta} c_0,$$

where $\alpha = v_{abc} / v_{ab}$ and $\beta = u_{abc} / u_{ab}$ are measured by experiments.

The ligation rate k is determined as follows. At small t , $[ab]_f = 0$, $[a]_f \approx [a]_0$, and $[b]_f \approx [b]_0$ because the template concentration $[\overline{cba}]_0 = 0.25$ nM is much smaller than $[a]_0 = 100$ nM and $[b]_0 = 33.3$ nM. By inserting these values, we obtain the reaction rates for the ligation of ab from $a + b$ and that of abc from a and bc :

$$k_{ab} \approx \frac{v_{ab}}{[\overline{cba}]_0} \left(1 + \frac{K_{D,20}}{[a]_0} + \frac{K_{D,20}}{[b]_0} \right) \quad \text{and} \quad k_{abc} \approx \frac{v_{abc}}{[\overline{cba}]_0} \left(1 + \frac{K_{D,20}}{[a]_0} + \frac{K_{D,40}}{[bc]_0} \right).$$

Figure S5b, d, and f shows the experimental ligation curves. From these curves, we obtained the values of the parameters $K_{D,20} = 193$ nM, $K_{D,40} = 4.5$ nM, $k_{ab} = 3.0$ nM⁻¹cycle⁻¹ and $k_{abc} = 3.0$ nM⁻¹cycle⁻¹. k_{ab} and k_{abc} were similar values. In the following simulations, we assumed that k is independent of the sequences of substrates and templates.

In case of (ii) and (iii), $K_{d,60}$ also affects the growth curves although it has no effect on v_{abc} and u_{abc} . By fitting the simulated curves with the parameters obtained above, we roughly estimated $K_{d,60}$ to be 2.7 nM.

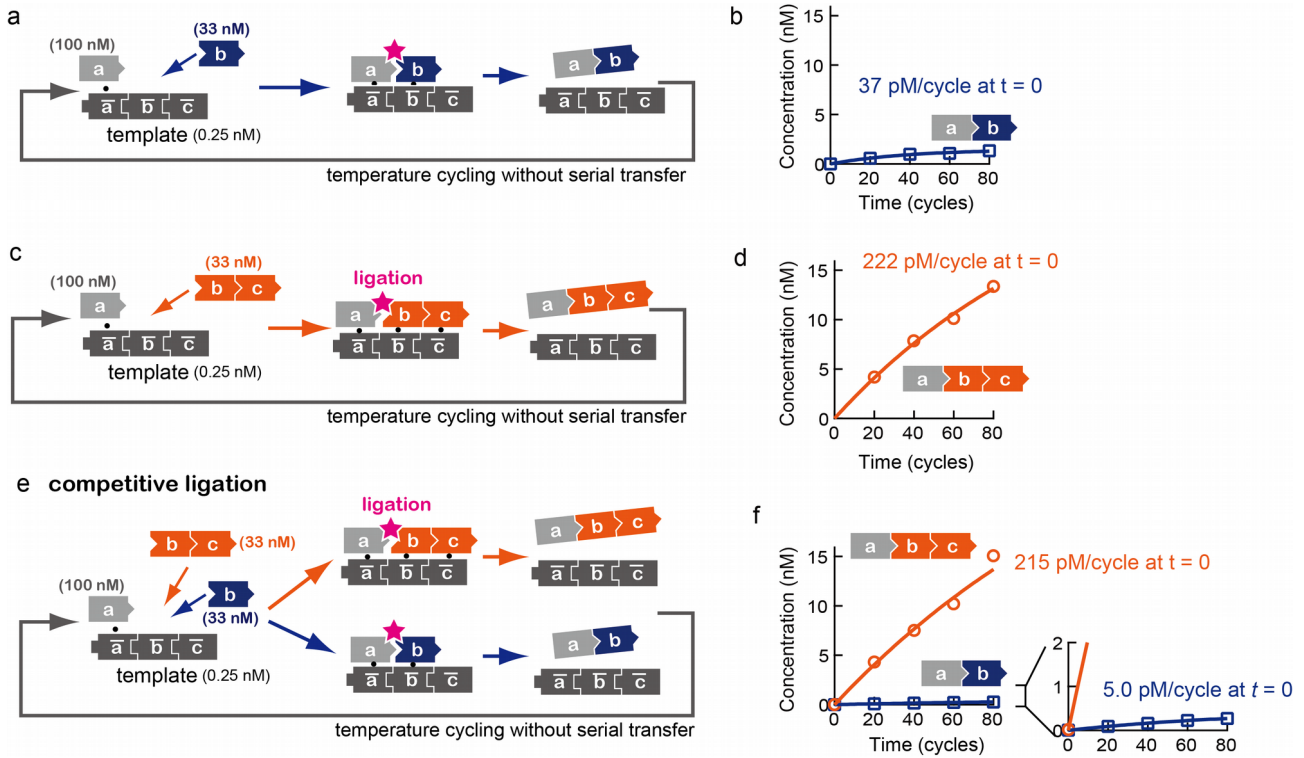


Figure S5: Linear ligation experiments for measuring the dissociation constants K_D the reaction rate k with various combinations of substrates. We performed thermal cycles between 67°C for 10s and 95°C for 5s without serial dilutions. For measuring the amounts of AB and ABC separately, we used a special longer substrate $bq = \text{ATGAG GGACA AGGCA ACAGT GAACT CAGTG TAGCC TCAGA T}$ for b . The sequence q does not hybridize to \bar{c} and is floating when b hybridizes to \bar{b} . See supplement S2 for the probing. The amount of each sequence was measured by COLD PCR^{S3}. The solid curves are obtained by simulation. **a**, **b**, Substrates are a and b . The ligation rate was 37 pM/cycle. **c**, **d**, Substrates are a and bc . The ligation rate was 222 pM/cycle. **e**, **f**, Substrates are a , b , and bc (competitive binding). The ligation rates of ABC and AB were 215 and 5.0 pM/cycle, respectively. We found that (i) dimers are ligated much faster than monomers. (ii) When dimers and monomers compete, ligation of monomers are suppressed substantially while the ligation of dimers are not significantly affected. 40-base strands are ligated about 43 times faster than monomers. Solid curves in **b**, **d**, and **f** are curves fitted by $y(t) = (v_0 / q) [1 - \exp(-qt)]$ with fitting parameters v_0 and q .

S4. Gel electrophoresis

Denaturing electrophoresis^{S5} was run at 400V for 15 min in 1x Tris-Borate-EDTA buffer (pH8) with denaturing polyacrylamide gels containing 12.5% acrylamide/bisacrylamide (19:1) and 50% urea (Carl Roth, Karlsruhe, Germany or WAKO, Japan). DNA strands were probed with a fluorescent dye 1x SYBR Gold (Thermo Fisher Scientific, MA, USA). The gel image was taken by a CCD camera on an UV transilluminator (Fig. S6) or an LED-illuminated gel documentation station (Fig. S7a) and analysed by lab-developed LabVIEW (National Instruments, USA) program. The pixel intensity data was projected to one dimensional intensity profile in the lane axis direction. Peaks in the profile were fitted by super-positions of Lorentzian functions to estimate the DNA amount contained in each band (Fig. 2b and S7b-e).

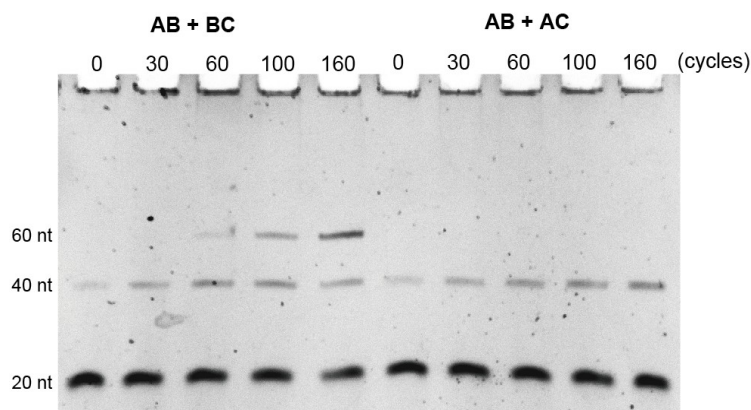


Figure S6: Measurement of length distribution of the strands. **a, b,** Electrophoresis gels stained with 1x SYBR Gold. The data correspond to the length distributions in Fig.2b

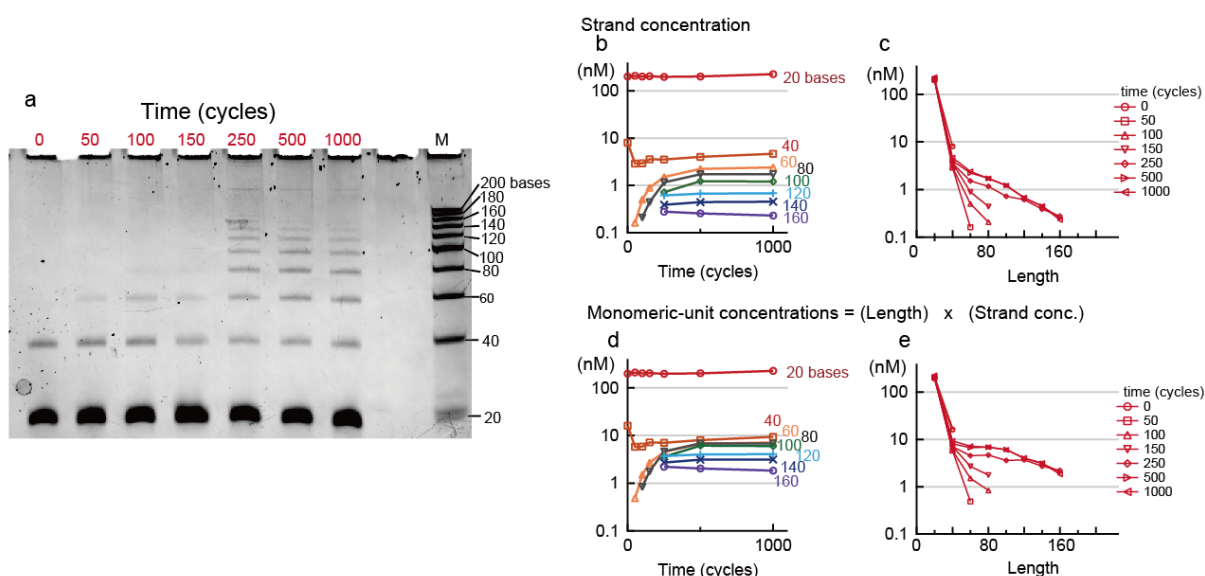


Figure S7: Measurement of length distribution of the strands. **a,** Electrophoresis gels stained with 1x SYBR Gold. The data correspond to the length distributions in Fig.4b. **b, c,** Strand concentrations. **d, e,** Mono-unit concentrations indicate how much mon-unit molecules are found in a given oligomer length.

S5. Numerical simulations

We solved deterministic differential equations on Mathematica 10.1 (Wolfram research, IL, USA). The equations include all the essential features of the experiments including the ligations, hybridizations between strands, conservation laws, and serial dilutions that feed substrates and dilute the products. The simulation parameters (dissociation constants and ligation rate) were determined by experiments (supplement S3). These parameters reproduced the experimental data well qualitatively. We modified the ligation rate to incorporate the effects of the limited amount of the ligase and the ligase degradation. The modified parameters reproduced the results quantitatively. The details will be described in the following. Because of the inherent symmetry in the system between (a, b, c) and $(\bar{a}, \bar{b}, \bar{c})$, it is not necessary to distinguish them in simulations. In the following, we use the notations (A, B, C) .

In experiments, we cycled temperatures. As cooled down to 67°C, hybridized complexes form and ligation reactions take place. As heated to 95°C, the ligated products and substrates dissociate from the template. It is not reasonable to simulate the step-wise hybridization and dissociation kinetics at high temperatures and to model the serial dilution in a discontinuous fashion. Instead, we solved differential equations of a continuous model. The simulation reproduced the experimental results well (Fig. 2, 3 and 4). Note that all concentrations are large enough such that stochastic simulations were not necessary and ordinary rate equations with concentrations were sufficient.

The continuous simulations were performed with approximations that (i) ligations take place at a constant rate from a complex containing neighboring hybridizations of substrates on a template and (ii) the complex formation is equilibrated with effective dissociation constants K_D determined by experiments (supplement S3). By solving the conservation laws of the strand concentrations, the complex concentration is determined. The ligation rate is the same independent of the substrate and template sequences (supplement S3). The serial dilution was implemented by explicit dilution and feeding process except Fig. 5 and S8. This will be explained later. In Fig. 5 and S8, the serial dilution was simulated with a constant degradation term with a dilution rate d .

Because it is not feasible to consider all the sequences to be involved in the reactions, we limited the maximum length of strands to 120 bases (Fig. 4a), 640 bases (Fig. 4b), or 80 bases (Fig. 5, S8). As evaluated with control simulations with shorter and longer strand lengths, the simulated lengths affect the results only insignificantly. In Fig. 4a, we did not observe a qualitative difference when we shortened the maximum length of the simulation. We did not find a clear tendency when the maximum length is varied. In Fig. 4a, for instance, the amount ratio between the majority and minority sequences at $t = 1200$ cycles were 443 with 80-base maximum, 781 with 100-base maximum length, and 538 with 120-base maximum length. In Fig. 4b, the affect of the change in the maximum length does not affect even quantitatively because the maximum length of 640-bases are sufficiently long and most strands contained are much shorter as seen in Fig. 4b. In Fig. 2b, 2c and 3, because the strands do not concatenate longer than 60 bases due to limited number of initial 40-base template strands, we simulated all possible sequences in the calculation.

We considered all the possible complexes containing up to three strands (Fig. 4, 5, and S8) or four strands (Fig. 2b, 2c and 3). This approximation is reasonable because the chance of a large complex formation is much smaller than the three- or four-body complexes. Hybridizations into large complexes tend to be composed of a combination of three- or four-body complexes and thus does not change the mechanisms qualitatively. Moreover, the larger the complex becomes, the longer time it takes to build the complex due to the limited diffusion time to assemble the complex. This kinetic disadvantage limits the concentration of a large complex in the present experimental system with the finite reaction time.

Still, with all of above, the resulting kinetic equations are still huge due to the large number of sequences. The size of the ASCII-file that contain the equation amounts to 30MB. We compiled a PDF with small font size of the whole equations solved and include in the supplement the Visual C#-source code that was used to generated the equations for Mathematica to solve. In order to understand the logic, we show for a short reaction system the parts of which the original equations were composed of:

Reactions:

$$\begin{aligned} [\dot{A}] &= -k' (2[A, A/AA] + [A, B/AB] + [A, BC/ABC] + [B, A/BA] + \dots) \\ [\dot{AB}] &= k' ([A, B/AB] + [A, B/CAB] + [A, B/ABC] + [A, B/ABB] + \dots) \\ &\quad - k' ([AB, C/ABC] + [AB, C/AB] + [A, AB/AA] + \dots) \\ [\dot{ABC}] &= k' ([AB, C/ABC] + [AB, C/AB] + [AB, C/BBC] + [A, BC/ABC] + [A, BC/AB] + [A, BC/CAB] + \dots) \\ &\quad - k' ([ABC, C/CC] - [A, ABC/AAB] + \dots) \end{aligned}$$

Here, terms like $[X / Y]$ are concentrations of hybridized duplex. Terms like $[X, Y / Z]$ are concentrations of hybridized triplex. For instance, $[A, B / ABC]$ corresponds to a complex with A and B hybridized on ABC. The concentrations of these complexes are determined by solving the following hybridization and conservation laws. We included the hybridizations with imperfect matching like $[AB, C / BBC]$, in which AB binds to BBC with only one overlap B. A does not bind to anywhere. Ligations take place only when the end sequences of the substrates (B and C in this case) are matched with the template sequences.

In experiments, we diluted by 1/6 every 50 thermal cycles. We included this serial dilution process in the simulations for Figs. 3 and 4. We did not explicitly include this effect in the simulations for Fig. 5 and S8, instead we performed a continuous simulation including dilution terms with a corresponding dilution rate $d = 0.036/\text{cycle}$. The feeding term $+ dm_0$ was added only to the reaction equations of monomers. m_0 is a feeding concentration of monomers and we used the values of the corresponding experiments.

k' is a reaction rate and independent of strand length and sequence. $k'(t) = \alpha k f_\tau(t)$. Here, k is determined by experiments (supplement S3) to be $3.0 \text{ nM}^{-1}\text{cycle}^{-1}$. The coefficient α corresponds to the modification due to the limiting amount of the ligase. When the DNA strands in the solution is high, the ligase that DNA strands can use is limited. Thus, the ligation rate decreases effectively with the amount of the DNA strands. The term $f_\tau(t)$ corresponds to the ligase degradation effect. At each serial dilution, fresh ligase will be put into the solution. We assumed that the ligase degrades exponentially with a time constant of τ . In the n -th round of serial dilutions, $f_n(t) = (1-p)e^{-(t-(n-1)t_0)/\tau} + pf_{n-1}(t)$, $f_1(t) = e^{-t/\tau}$ where p is a dilution ratio at each dilution ($= 1/6$), and $t_0 = 50$ cycles is the period between succeeding serial dilutions. We found that $\tau = 80$ cycles reproduced the experimental data well. This is a reasonable length for the thermostable DNA ligase.

Hybridizations:

As noted, we calculated the hybridized complex concentrations by using the equilibrium binding expressions with the effective dissociation constants $K_{D,n}$ to reduce the computational cost. $K_{D,n}$ corresponds to the hybridization with a n -base overlap. We determined $K_{D,20}$, $K_{D,40}$, and $K_{D,60}$ by experiments (supplement S3). For the overlap longer than 60 bases, we used the same value as $K_{D,60}$ ($K_{D,n} = K_{D,60}$ for $n > 60$). This is a reasonable assumption by the binding thermodynamics. Complex concentrations were calculated by, for instance,

$$[A/AB] = \frac{[A]_f [AB]_f}{K_{D,20}}, \quad [AB, C/ABC] = \frac{[AB]_f [C]_f [ABC]_f}{K_{D,40} K_{D,20}}, \quad [AB, C/A, BC] = \frac{[AB]_f [C]_f [A]_f [BC]_f}{K_{D,20} K_{D,20} K_{D,20}}.$$

Here, $[\]_f$ denotes the concentration of the free strand. $[AB, C / A, BC]$ denotes a four-body complex where AB and BC are hybridized with overhangs, and C and A are hybridized to these overhangs. Some complexes have isomers, that is, they have the same compositions but have different hybridization shapes. For example, AA can hybridize to AAC in two ways; one with only 20-base overlap and an overhang and one with 40-base overlap and no overhang. We differentiated these isomers:

$$[AA/AAC]^{(1)} = \frac{[AA]_f [AAC]_f}{K_{D,20}}, \quad [AA/AAC]^{(2)} = \frac{[AA]_f [AAC]_f}{K_{D,40}}.$$

As noted, we included the hybridizations with imperfect matching. We counted the overlap length only in the region with the matching. For example, ABC/ACC has only 40-base overlap in total. Therefore, we use $K_{D,40}$ for this hybridization.

$$[AC/AB] = \frac{[AC]_f [AB]_f}{K_{D,20}}, \quad [ABC/ACC] = \frac{[ABC]_f [ACC]_f}{K_{D,40}}, \quad [AB, C/BBC] = \frac{[AB]_f [C]_f [BBC]_f}{K_{D,20} K_{D,20}}.$$

Conservation laws:

The following conservation laws were solved with the above hybridization expressions to obtain the free concentrations of strands such as $[A]_f$ and $[AB]_f$. This determines the complex concentrations necessary in the reaction equations.

$$[A] = [A]_f + [A/A] + [A/AB] + [A/CA] + [A/BAC] + \dots + [A, B/AB] + [A, BC/ABC] + [C, A/CBA] + \dots$$

$$[AB] = [AB]_f + [A/AB] + [AB/AB] + [A/CA] + \dots + [A, B/AB] + [AB, C/ABC] + 2[AB, AB/ABAB] + \dots$$

In the first line, $[A / A]$ contains two A. However, A should not be counted twice because of a symmetric reason. Therefore, coefficient 2 is not necessary in front of $[A / A]$. As noted, we differentiated isomeric complexes. The parameters (reaction rate k and dissociation constants $K_{D,20}$, $K_{D,40}$, and $K_{D,60}$) were obtained by experiments (Fig. S5): $K_{D,20} = 193 \text{ nM}$, $K_{D,40} = 4.5 \text{ nM}$, $K_{D,60} = 2.7 \text{ nM}$, and $k = 3.0 \text{ nM}^{-1}\text{cycle}^{-1}$. We assumed $K_{D,n} = K_{D,60}$ for $n > 60$ for simplicity since longer strands $n > 60$ were estimated to yield a similarly large high

probability to bind to a matching strand than the 60 bases. The simulation details vary according to the corresponding experiments as follows.

Serial dilution:

The serial dilution was implemented as follows except Fig. 5 and S8. (i) Continuous simulation was performed for 50 cycles. (ii) The strand concentrations were diluted by 1/6 except 20mer strands; $[X] \rightarrow 1/6 [X]$. 20mer strands were not only diluted but also fed; $[X] \rightarrow 1/6 [X] + 5/6 X_0$, where $X_0 = 33.3$ nM is the feeding concentration of 20mer substrates. (iii) With these updated values as the initial strand concentrations, we repeated (i) and (ii).

Because such an explicit implementation of serial dilutions was not feasible in Fig. 5 and S8, we simulated the serial dilution with a continuous degradation of 3.6% / cycle ($= 1 - (1/6)^{1/50}$).

5.1 Cooperative ligation (Fig. 2b and 2c).

Because the strands do not elongate longer than 60 bases due to limited number of initial 40-base template strands, the model equations are relatively simple. To test and for completeness, not only the three-body binding, but also four-body bindings were calculated. Including these computationally very elaborate, but in the reaction not very significant complexes did not affect the results significantly. Apparently, they are well enough covered by the modeling of the dimeric binding kinetics. The solved equations in the Mathematica (Wolfram) form is shown below.

(* Reactions *)

```
a0'[t] == k[t] (-a[t]b[t]ab[t] - a[t]bc[t]ab[t] - a[t]c[t]ac[t] - a[t]b[t]abc[t] -
a[t]bc[t]abc[t]*r2)*r1*r1 + (-a[t]b[t]c[t]abc[t] - ab[t]c[t]a[t]bc[t])*r1*r1*r1,
b0'[t] == k[t] (-a[t]b[t]ab[t] - b[t]c[t]bc[t] - a[t]b[t]abc[t] - b[t]c[t]abc[t])*r1*r1 + (-
2a[t]b[t]c[t]abc[t])*r1*r1*r1 - db0[t],
c0'[t] == k[t] (-a[t]c[t]ac[t] - b[t]c[t]bc[t] - ab[t]c[t]bc[t] - b[t]c[t]abc[t] -
ab[t]c[t]abc[t]*r2)*r1*r1 + (-a[t]b[t]c[t]abc[t] - a[t]bc[t]ab[t]c[t])*r1*r1*r1,

ab0'[t] == k[t] (+a[t]b[t]ab[t] - ab[t]c[t]bc[t] + a[t]b[t]abc[t] - ab[t]c[t]abc[t]*r2)*r1*r1 +
(a[t]b[t]c[t]abc[t] - a[t]bc[t]ab[t]c[t])*r1*r1*r1,
ac0'[t] == k[t] (+a[t]c[t]ac[t])*r1*r1,
bc0'[t] == k[t] (-a[t]bc[t]ab[t] + b[t]c[t]bc[t] - a[t]bc[t]abc[t]*r2 + b[t]c[t]abc[t])*r1*r1 +
(a[t]b[t]c[t]abc[t] - ab[t]c[t]a[t]bc[t])*r1*r1*r1,

abc0'[t] == k[t] (+a[t]bc[t]ab[t] + ab[t]c[t]bc[t] + a[t]bc[t]abc[t]*r2 + ab[t]c[t]abc[t]*r2)*r1*r1 +
(a[t]bc[t]ab[t]c[t] + ab[t]c[t]a[t]bc[t])*r1*r1*r1,
```

(* Conservation laws *)

```
a0[t] == a[t] + (+a[t]a[t] + a[t]ab[t] + a[t]ac[t] + a[t]abc[t])*r1 + (+a[t]b[t]ab[t] + a[t]bc[t]ab[t]
+a[t]c[t]ac[t] + a[t]b[t]abc[t] + a[t]c[t]abc[t] + a[t]ac[t]abc[t] + a[t]bc[t]abc[t]*r2)*r1*r1 +
(a[t]b[t]c[t]abc[t] + ab[t]c[t]a[t]bc[t])*r1*r1*r1,
b0[t] == b[t] + (+b[t]b[t] + b[t]ab[t] + b[t]bc[t] + b[t]abc[t])*r1 + (+a[t]b[t]ab[t] + b[t]c[t]bc[t]
+a[t]b[t]abc[t] + b[t]c[t]abc[t])*r1*r1,
c0[t] == c[t] + (+c[t]c[t] + c[t]ac[t] + c[t]bc[t] + c[t]abc[t])*r1 + (+a[t]c[t]ac[t] + b[t]c[t]bc[t]
+ab[t]c[t]bc[t] + a[t]c[t]abc[t] + b[t]c[t]abc[t] + ab[t]c[t]abc[t]*r2 + ac[t]c[t]abc[t])*r1*r1 +
(a[t]b[t]c[t]abc[t] + a[t]bc[t]ab[t]c[t])*r1*r1*r1,

ab0[t] == ab[t] + (+a[t]ab[t] + b[t]ab[t] + ab[t]ab[t]*r2 + ac[t]ab[t] + bc[t]ab[t] + ab[t]abc[t]*r2)*r1 +
(+ab[t]c[t]bc[t] + a[t]b[t]ab[t] + a[t]bc[t]ab[t] + ab[t]c[t]abc[t]*r2)*r1*r1 + a[t]bc[t]ab[t]c[t]*r1*r1*r1,
ac0[t] == ac[t] + (+a[t]ac[t] + c[t]ac[t] + ab[t]ac[t] + ac[t]ac[t]*r2 + bc[t]ac[t] + ac[t]abc[t]
+ac[t]abc[t])*r1 + (+a[t]c[t]ac[t] + a[t]ac[t]abc[t] + ac[t]c[t]abc[t])*r1*r1,
bc0[t] == bc[t] + (+b[t]bc[t] + c[t]bc[t] + ab[t]bc[t] + ac[t]bc[t]*r2 + bc[t]abc[t]*r2)*r1 +
(+a[t]bc[t]ab[t] + b[t]c[t]bc[t] + ab[t]c[t]bc[t] + a[t]bc[t]abc[t]*r2)*r1*r1 + ab[t]c[t]a[t]bc[t]*r1*r1*r1,

abc0[t] == abc[t] + (+a[t]abc[t] + b[t]abc[t] + c[t]abc[t] + ab[t]abc[t]*r2 + ac[t]abc[t] + ac[t]abc[t]
+bc[t]abc[t]*r2 + abc[t]abc[t]*r3)*r1 + (+a[t]b[t]abc[t] + a[t]c[t]abc[t] + a[t]ac[t]abc[t]
+a[t]bc[t]abc[t]*r2 + b[t]c[t]abc[t] + ab[t]c[t]abc[t]*r2 + ac[t]c[t]abc[t])*r1*r1 +
a[t]b[t]c[t]abc[t])*r1*r1*r1
```

Here, $a[t]$, $b[t]$... are the concentrations of the free strands. $a0[t]$, $b0[t]$ are the total concentrations of the strands. $r1 = 1/k_{D,20}$, $r2 = k_{D,20}/k_{D,40}$, $r3 = k_{D,20}/k_{D,60}$. The ligation rate $k[t]$ is $k_0 \text{Exp}[-t/80]$ with $k_0 = 3.0$ nM/s.

In Fig. 2c, we plot $\langle AB \rangle = 2(ab0[t] + abc0[t])$, $\langle BC \rangle = 2(bc0[t] + abc0[t])$, and $\langle AC \rangle = 2(ac0[t])$ for the simulation curves in “PCR” plots, and monomers = $2(a0[t] + b0[t] + c0[t])$, dimers = $2(ab0[t] + bc0[t] + ac0[t])$, and trimers = $2abc0[t]$ for the simulation curves in “Gel” plots.

5.2 Selection by cooperation (Fig. 3).

Because the strands do not elongate longer than 60 bases due to limited number of initial 40-base template strands, the model equations are relatively simple. To test and for completeness, not only the three-body binding, but also four-body bindings were calculated. Including these computationally very elaborate, but in the reaction not very significant complexes did not affect the results significantly. Apparently, they are well enough covered by the modeling of the dimeric binding kinetics.

For Fig. 3d, we biased k_D so that A and B bind more stably than C. More specifically, k_D was biased as $\sqrt{m}k_D$ for the hybridization including A and B, and $\sqrt{1/m}k_D$ for the hybridization including C. Here, the parameter m is the number indicated in Fig. 3d as 1.3, 2, 3, and 4 fold. If the hybridization contains multiple units, we multiply all the biases. For example, the k_D of a complex with the hybridization of A and BC on ABC, the dissociation constant of this complex becomes $\sqrt{m}\sqrt{m}\sqrt{1/m}k_{D,20}k_{D,40} = \sqrt{m}k_{D,20}k_{D,40}$.

5.3 Domination by the majority sequence motifs (Fig. 4a).

We used the additional symmetries such as $[AB] = [BC] = [CA]$ and $[CB] = [BA] = [AC]$ for reducing the computational time without affecting the results. Since the number of possible sequences grow exponentially with the length, we restricted the maximum length to six and neglected the reactions that produce strands longer than 120 bases in order to suppress the computational time. As shown before, the four-body bindings which are computationally very expensive are not expected to significantly affect the results and were not calculated.

5.4 Length distribution (Fig. 4b).

The simulation results indicated that the length distribution is mostly determined by the dominant sequences. Thus, considering only reactions including sequence motifs AB, BC, and CA, the number of reaction terms decrease dramatically and the prediction of the length distribution is not significantly affected. We calculated the length distribution by using terms of up to a length of 640 bases (32 units).

5.5 Symmetry breaking (Fig. S9) and spatial pattern formation (Fig. 5, S8)

We started the simulations in Fig. S9, S8 and Fig. 5 with uniform concentrations of all the nine dimer templates with 5% concentration fluctuations. We restricted the maximum length to 80 bases and neglected the reactions that produce strands longer than 80 bases in order to reduce the computational time. Again, four-body bindings were not considered. The dilution rate was $d = 0.045$ /cycle. This slightly higher value than experiments was used because this provided better splitting.

S6. Stochastic emergence of self-sustaining sequence structure

For the one-dimensional simulations in Fig. 5 and S8, diffusion terms such as $D\partial^2[A]/\partial x^2$ are incorporated into all the reaction equations. Here, D is a diffusion coefficient and is independent of sequence and strand length for simplicity. We used a periodic boundary condition. In the simulations, we find the following six patterns of collaboration with the used three sequences if the cooperation is active (Fig. S8):

-	Periodic	patterns	with	three	letters:
AB,BC,CA				...ABC...	
AC,BA,CB		→			
-	Periodic	patterns	with	two	letters
BC,CB,AA				...BCBC...	and
AC,CA,BB		→		...ACAC...	and
AB,BA,CC		→		...ABAB... and ...CCC...	and
					homogeneous
-	The	completely		homogeneous	case:
AA,BB,CC		→		...AAA..., ...BBB... and ...CCC...	

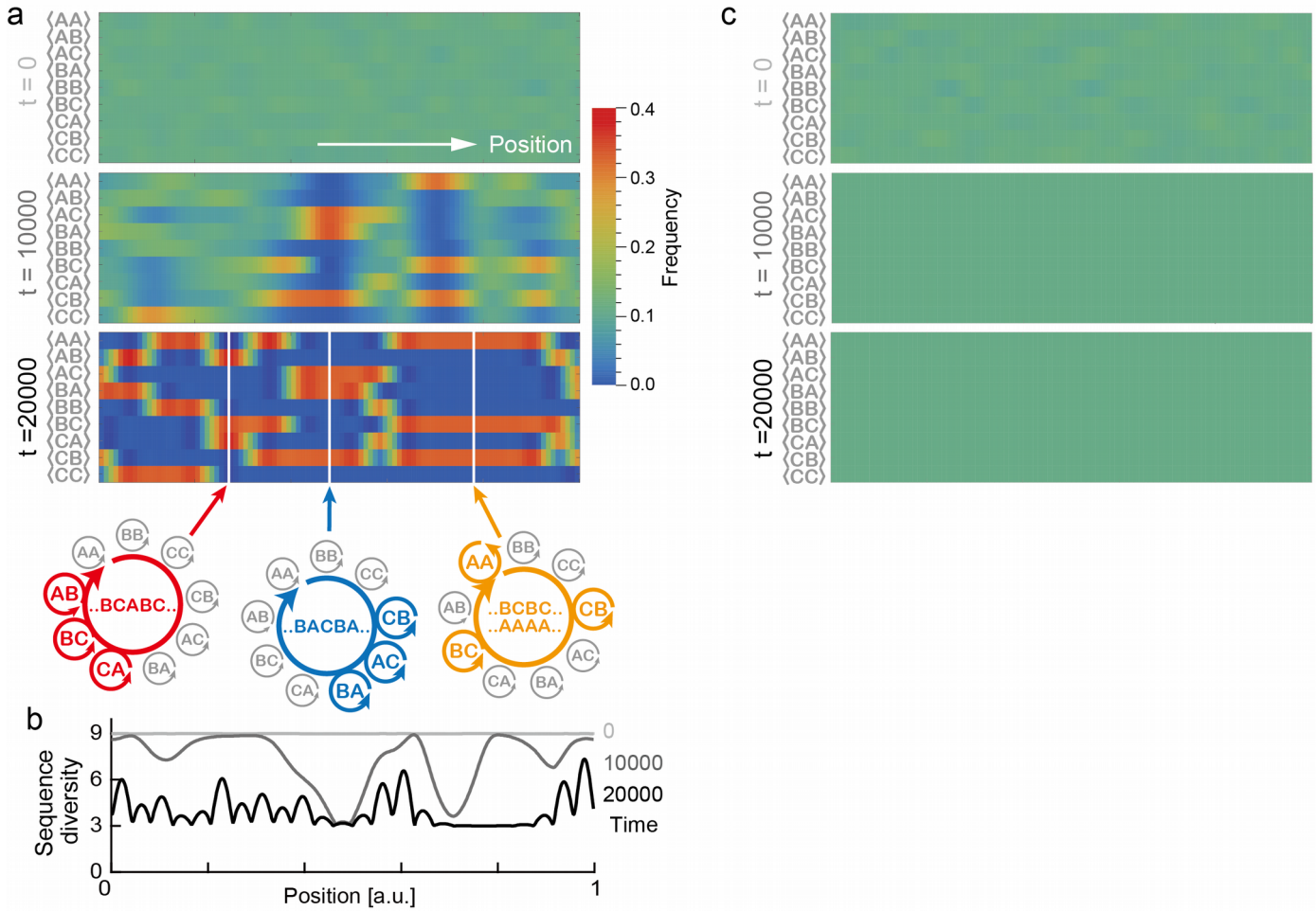


Figure S8: **a**, Same as Fig. 5 but reproduced for the comparison with the sequence entropy (**b**) and the non-cooperative condition (**c**). **b**, The sequence diversity is plotted as a function of position. The sequence diversity is quantified by the exponential of the Shannon entropy $\exp(-\sum_i p_i \ln p_i)$ with p_i the frequency of i -th dimeric sequence motif. Approximately, this amounts to the number of dominant two-letter motifs. Here, diffusion coefficient was set to 10^{-7} /cycle. The experimental value depends on the length but is about 10^{-9} cm^2/s ³³. Comparing these two values with assuming that one cycle takes 30 seconds, the whole horizontal range shown in **a** and **b** corresponds to approximately 5 mm. **c**, Same as **a** but under a non-cooperative condition $K_{D,20} = K_{D,40} = K_{D,60}$ ($= 150$ nM). The initial concentration fluctuations disappear soon, and the system converges into a uniform state instead of forming a spatial pattern.

Below in Figure S9, we present simulation runs with a homogeneously mixed solution. As can be seen, the system amplifies the stochastic initial conditions with 5% variations in concentration to emerge above cooperating two letter sequences. We find the six classes of cooperation as indicated above. Of course it would interesting to see how which cooperating sequences would emerge from complex sequence starting conditions, but this is left for future studies.

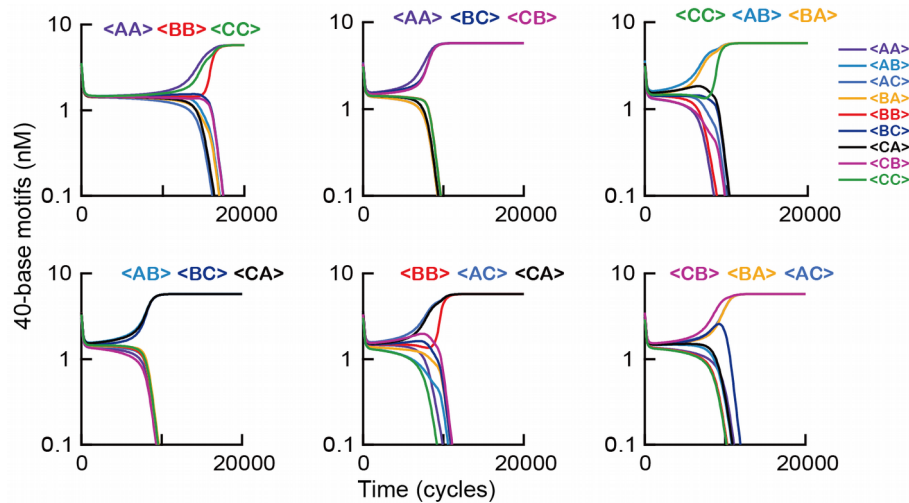


Figure S9: Stochastic emergence of sequence structures is observed when we initiated the reactions by a uniform concentration of all the nine possible dimers (AA, AB, ..., CC) with 5% concentration fluctuations. We observed a state dominated by one of six possible cooperative combinations. For example, AB and AC do not coexist because AB and AC are competitive; B and C compete to get the right hand side of A. The dilution rate is $d = 0.045$ / cycle.

S7. Theoretical analysis

The mechanism of the higher-order growth by the cooperation and the frequency-dependent separation is theoretically studied here.

7.1 Nonlinear cooperative growth

The set of equations used in the simulation (S5) is huge. Instead, we use a simpler model. Think of a simple cooperative system with the templates AB and BC. This corresponds to the experiment shown in Fig. 2 (Cooperative Ligation in 2b and 2c). The rate equations are

$$\begin{aligned}\dot{[A]} &= -k'([A][B]([AB] + [ABC]) + [A][BC]([AB] + (1+p)[ABC])) - d([A] - S), \\ \dot{[B]} &= -k'([A][B]([AB] + [ABC]) + [B][C]([BC] + [ABC])) - d([B] - S), \\ \dot{[C]} &= -k'([B][C]([BC] + [ABC]) + [AB][C]([BC] + (1+p)[ABC])) - d([C] - S), \\ \dot{[AB]} &= k'([A][B]([AB] + [ABC]) - [AB][C]([BC] - (1+p)[AB][C][ABC])) - d[AB], \\ \dot{[BC]} &= k'([B][C]([BC] + [ABC]) - [A][BC][AB] - (1+p)[A][BC][ABC]) - d[BC], \\ \dot{[ABC]} &= k'([A][BC][AB] + [AB][C][BC] + (1+p)[A][BC][ABC] + (1+p)[AB][C][ABC]) - d[ABC].\end{aligned}$$

Here, $k' \equiv k/K_{D,20}^2$ and $p \equiv K_{D,20}/K_{D,40-1} - 1$. We omit the hybridization for simplicity. This does not affect the qualitative results in the following.

With arrangements, we obtain the rate equations of the sequence motifs $\langle AB \rangle \equiv [AB] + [ABC]$ and $\langle BC \rangle \equiv [BC] + [ABC]$:

$$\begin{aligned}\dot{\langle AB \rangle} &= k'[A]([B_L]\langle AB \rangle + p[BC][ABC]) - d\langle AB \rangle, \\ \dot{\langle BC \rangle} &= k'[C]([B_R]\langle BC \rangle + p[AB][ABC]) - d\langle BC \rangle, \\ \dot{[A]} &= -k'[A]([B_L]\langle AB \rangle + p[BC][ABC]) - d([A] - S), \\ \dot{[B_L]} &= -k'[A]([B_L]\langle AB \rangle + p[BC][ABC]) - d([B_L] - S), \\ \dot{[B_R]} &= -k'[C]([B_R]\langle BC \rangle + p[AB][ABC]) - d([B_R] - S), \\ \dot{[C]} &= -k'[C]([B_R]\langle BC \rangle + p[AB][ABC]) - d([C] - S).\end{aligned} \quad \dots (7.1.1)$$

$[B_L] \equiv [B] + [BC]$ and $[B_R] \equiv [B] + [AB]$ are the amount of the strands with B at the most left and B at the most right in the sequence, respectively. (7.1.1) clarifies that B_L and B_R serve as the substrates for the AB connection ($A + B \rightarrow AB$ and $A + BC \rightarrow ABC$) and BC connection ($B + C \rightarrow BC$ and $AB + C \rightarrow ABC$), respectively. S is the amount of the substrate supply. The parameter p indicates the strength of the nonlinear cooperative term $p k'[A][BC][ABC]$ and $p k'[AB][C][ABC]$.

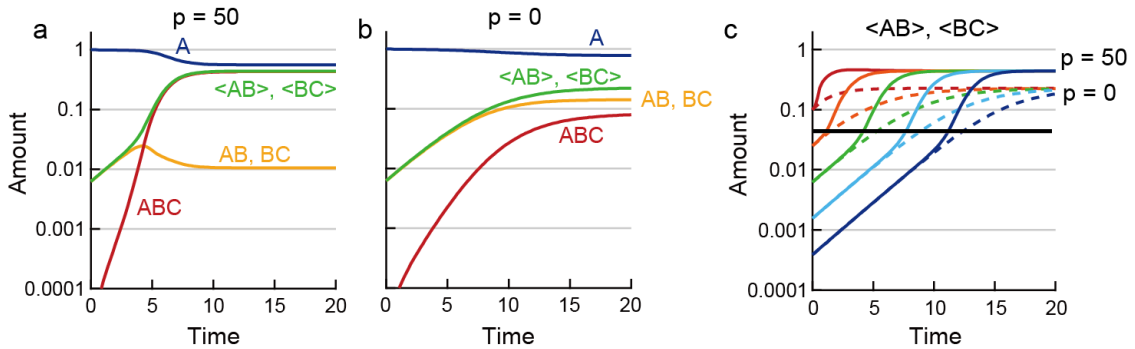


Fig. S10. Simulation curves of (7.1.1) with the parameters $k' = 1$, $d = 0.6$, $S = 1$, and $p = 0$ or 50 . The initial conditions are $A(0) = B(0) = C(0) = 1$. $ABC(0) = 0$. $AB(0) = BC(0) = 0.1 / 16$ in **a** and **b** and 0.1 (red), $0.1 / 4$ (orange), $0.1 / 16$ (green), $0.1 / 64$ (cyan), $0.1 / 256$ (navy) in **c**. **a**, Growth curves of A (navy), AB , BC (orange), ABC (red), and $\langle AB \rangle = AB + ABC$, $\langle BC \rangle = BC + ABC$ (green) with positive cooperativity ($p = 50$). The initial amounts of **b**, Same as **a** but $p = 0$. **c**, Simulation curves of $\langle AB \rangle$ and $\langle BC \rangle$ for different initial concentrations of AB and BC with $p = 50$ (solid lines) and 0 (dashed lines). The curves show that the growth is accelerated at a specific amount of $\langle AB \rangle$ and $\langle BC \rangle$ indicated by a horizontal black thick line, which does not depend on the initial amount.

The equations (7.1.1) are simulated in Fig. S10. With positive p (Fig. S10a), AB and BC accumulate in the early

stages. Then, along with the growth of ABC, the growth of $\langle AB \rangle$ and $\langle BC \rangle$ accelerates. This higher-order growth is seen in the downward convex of the $\langle AB \rangle$ and $\langle BC \rangle$ curves. This demonstrates the positive feedback mechanism by the cooperation. The growth of $\langle AB \rangle$ and $\langle BC \rangle$ accumulates a longer strand ABC. This ABC mediates the cooperation between AB and BC and accelerates the growth. The above mechanism is further demonstrated in Fig. S10c. There is a threshold level (indicated by a black thin line) independent of the initial amount where the growth acceleration starts.

Without the cooperation (Fig. S10b), such a higher-order growth is not observed. Actually, with $p=0$, it is a simple first-order autocatalytic system with an exponential growth limited by the substrate depletion:

$$\begin{aligned}\dot{\langle AB \rangle} &= k' [A][B_L] \langle AB \rangle - d \langle AB \rangle, \\ \dot{\langle BC \rangle} &= k' [C][B_R] \langle BC \rangle - d \langle BC \rangle, \\ \dot{[A]} &= -k' [A][B_L] \langle AB \rangle - d([A] - S), \\ \dot{[B_L]} &= -k' [A][B_L] \langle AB \rangle - d([B_L] - S), \\ \dot{[B_R]} &= -k' [C][B_R] \langle BC \rangle - d([B_R] - S), \\ \dot{[C]} &= -k' [C][B_R] \langle BC \rangle - d([C] - S).\end{aligned}$$

Thus, p defined based on the K_D ratio determines if the higher-order growth takes place. The two factors; (i) The cooperation mediated by a longer strand and (ii) the ligation is faster with a longer overlapping account for the higher-growth.

7.2 Competition between two sequence motifs

To discuss the competition between the sequence motifs, we further simplify the above equations into a general autocatalytic system with a nonlinear term. Think of two competitive sequence motifs α and β sharing the same substrate:

$$\begin{pmatrix} \dot{\alpha} \\ \dot{\beta} \end{pmatrix} = k(S - \alpha - \beta) \begin{pmatrix} \alpha + p\alpha^2 \\ \beta + p\beta^2 \end{pmatrix} - d \begin{pmatrix} \alpha \\ \beta \end{pmatrix} \equiv \begin{pmatrix} f_\alpha(\alpha, \beta) \\ f_\beta(\alpha, \beta) \end{pmatrix} \quad \dots (7.2.1)$$

For example, α and β correspond to $\{\langle AB \rangle, \langle BC \rangle, \text{ and } \langle CA \rangle\}$ and $\{\langle CB \rangle, \langle BA \rangle, \text{ and } \langle AC \rangle\}$, respectively, in Fig. 4a. $S - \alpha - \beta$ is the amount of the substrates.

We do a standard linear-stability analysis to study the equations. The steady state is obtained by solving, or $\alpha_0[k(S - \alpha_0 - \beta_0)(1 + p\alpha_0) - d] = 0$ and $\beta_0[k(S - \alpha_0 - \beta_0)(1 + p\beta_0) - d] = 0$. There are three possible solutions;

- (i) $\alpha_0 = \beta_0 = 0$ (Trivial fixed point),
- (ii) $\{\alpha_0 = 0, \beta_0 \neq 0\}$ or $\{\alpha \neq 0, \beta = 0\}$ (Splitting), and
- (iii) $\alpha_0 = \beta_0 \neq 0$ (Uniform state).

The stability of these steady states against a small perturbation are determined by the sign of the eigenvalues of the Jacob matrix. If all the eigenvalues are negative, the state is stable. If the eigenvalues contain a positive value, the state is unstable and is not realized. The Jacob matrix at the steady state is

$$\begin{aligned}J(\alpha_0, \beta_0) &= \begin{pmatrix} \partial_\alpha f_\alpha(\alpha_0, \beta_0) & \partial_\beta f_\alpha(\alpha_0, \beta_0) \\ \partial_\alpha f_\beta(\alpha_0, \beta_0) & \partial_\beta f_\beta(\alpha_0, \beta_0) \end{pmatrix} \\ &= \begin{pmatrix} -k\alpha_0(1 + p\alpha_0) + k(S - \alpha_0 - \beta_0)(1 + 2p\alpha_0) - d & -k\alpha_0(1 + p\alpha_0) \\ -k\beta_0(1 + p\beta_0) & -k\beta_0(1 + p\beta_0) + k(S - \alpha_0 - \beta_0)(1 + 2p\beta_0) - d \end{pmatrix}\end{aligned}$$

Then, to know when the frequency-dependent selection takes place, we check the condition that the uniform state becomes unstable by a linear-stability analysis around the uniform state.

Using $k(S - \alpha_0 - \beta_0)(1 + p\alpha_0) = k(S - \alpha_0 - \beta_0)(1 + p\beta_0) = d$,

$$J(\alpha_0, \beta_0) = k \begin{pmatrix} -(\alpha_0 + p\alpha_0^2) + (S - \alpha_0 - \beta_0)p\alpha_0 & -(\alpha_0 + p\alpha_0^2) \\ -(\beta_0 + p\beta_0^2) & -(\beta_0 + p\beta_0^2) + (S - \alpha_0 - \beta_0)p\beta_0 \end{pmatrix}.$$

The eigen values of $J(\alpha_0, \beta_0)$ are $\lambda_1 = kp\alpha_0(S - 2\alpha_0)$ and $\lambda_2 = k\alpha_0(-2 - 4p\alpha_0 + pS) = \lambda_1 - 2k(\alpha_0 + p\alpha_0^2)$. The sign of the cooperativity p determines the stability of the

uniform state. If $p > 0$ (positive cooperation, hyperexponential growth), uniform state is unstable because $\lambda_1 > 0$. Separation takes place. If $p = 0$ (no cooperation, exponential growth), uniform state is neutral because $\lambda_1 = 0$ and $\lambda_2 = -2k\alpha_0 < 0$.

If $p < 0$ (negative cooperation, subexponential growth), uniform state is stable because $\lambda_1 < 0$ and $\lambda_2 = \lambda_2 - 2k(\alpha_0 + p\alpha_0^2) < \lambda_1 < 0$. Such the negative cooperation is possible if the product inhibition is strong. The motifs with lower frequency have higher growth rate. The curves simulated by (7.2.1) are shown in Fig. S11.

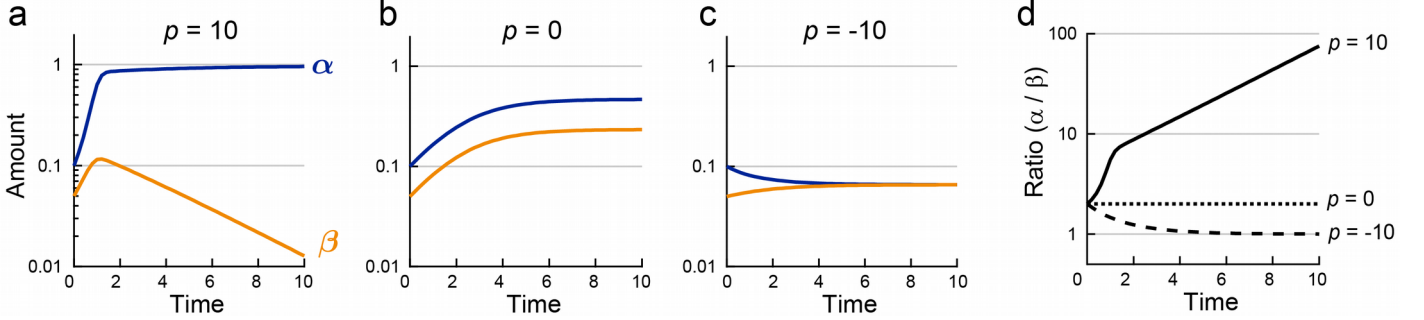


Fig. S11. The equations (7.2.1) are numerically solved with the parameters $k = 1$, $S = 1$, $d = 0.5$, and different values of p indicated. The initial conditions are $\alpha(0) = 0.1$ and $\beta(0) = 0.05$. (a – c) The amount of the two sequence motifs $\alpha(t)$ and $\beta(t)$. (a) If $p > 0$, the uniform state ($\alpha = \beta$) is unstable, and α and β split. α is selected because α has a higher initial amount than β . (b) If $p = 0$, the initial bias is kept. (c) If $p < 0$, the uniform state is stable. (d) The ratio of α to β .

The above analysis clarifies that the nonlinearity by cooperation demonstrated experimentally in Fig. 2c drives the frequency-dependent selection demonstrated experimentally in Fig. 4a.

7.3 One dimensional system

To discuss the pattern formation observed in the simulation (Fig. 5), we add a diffusional term to the above model.

$$\frac{\partial}{\partial t} \begin{pmatrix} \alpha(x, t) \\ \beta(x, t) \end{pmatrix} = k(S - \alpha - \beta) \begin{pmatrix} \alpha + p\alpha^2 \\ \beta + p\beta^2 \end{pmatrix} - d \begin{pmatrix} \alpha \\ \beta \end{pmatrix} + D \frac{\partial^2}{\partial x^2} \begin{pmatrix} \alpha \\ \beta \end{pmatrix} \quad \cdots (7.3.1)$$

Here, D is a diffusion coefficient. Linearized equations are

$$\frac{\partial}{\partial t} \begin{pmatrix} \alpha \\ \beta \end{pmatrix} = J(a_0, b_0) \begin{pmatrix} \alpha \\ \beta \end{pmatrix} + D \frac{\partial^2}{\partial x^2} \begin{pmatrix} \alpha \\ \beta \end{pmatrix}.$$

By inserting the perturbation around the steady state

$$\begin{pmatrix} \Delta_\alpha(x, t) \\ \Delta_\beta(x, t) \end{pmatrix} \equiv \begin{pmatrix} \alpha(x, t) - \alpha_0 \\ \beta(x, t) - \beta_0 \end{pmatrix} = e^{\lambda_q t + i q x} \begin{pmatrix} \alpha_0 \\ \beta_0 \end{pmatrix},$$

we obtain the following equation

$$\lambda_q \begin{pmatrix} \alpha_0 \\ \beta_0 \end{pmatrix} = \left[J(\alpha_0, \beta_0) - q^2 D \begin{pmatrix} 1 & 0 \\ 0 & 1 \end{pmatrix} \right] \begin{pmatrix} \alpha_0 \\ \beta_0 \end{pmatrix}.$$

The eigenvalues of $J(\alpha_0, \beta_0) - q^2 D \begin{pmatrix} 1 & 0 \\ 0 & 1 \end{pmatrix}$ are $\lambda_1 - Dq^2$ and $\lambda_2 - Dq^2$. The sign of these eigenvalues determine the stability of the uniform state and varied depending on the wave number q . When $p > 0$, stability of the uniform state is determined by the sign of $\lambda_2 - Dq^2 = kp\alpha_0(S - 2\alpha_0) - Dq^2$ because $\lambda_1 = \lambda_2 - 2k(\alpha_0 + p\alpha_0^2) - Dq^2$ is always smaller than λ_2 . In the wave-number range of

$q < q_{\max} \equiv \sqrt{\frac{kp\alpha_0(S - 2\alpha_0)}{D}}$, uniform state is unstable and a spatial pattern forms spontaneously. This

inequality reasonably suggests that the pattern becomes finer with smaller diffusion and larger reaction rate. Fig. S12 shows an example of the pattern formation simulated by (7.3.1) with different p . This demonstrates

that the pattern formation does not take place without a cooperation (Fig. S12b) as seen in Fig. S8.

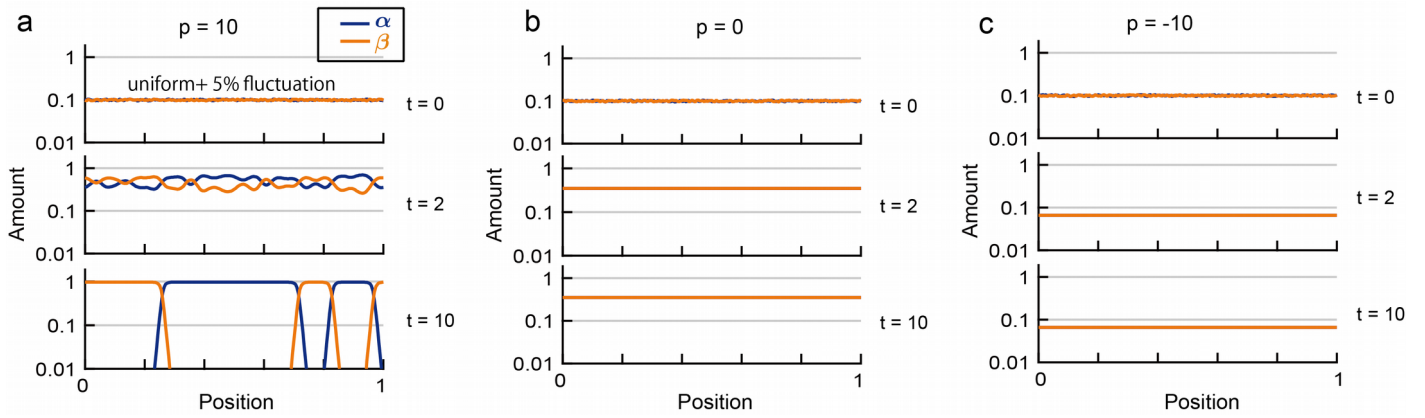


Fig. S12. The equations (7.3.1) are numerically solved with the parameters $k = 1$, $S = 1$, $d = 0.5$, and different values of p indicated. The initial conditions are 0.1 with 5% fluctuations picked from a uniform distribution. **(a – c)** The snapshots of the concentration profiles of $\alpha(x, t)$ and $\beta(x, t)$ are shown at $t = 0, 2, 10$. **(a)** If $p > 0$, the uniform state is unstable, and a spatial pattern forms spontaneously. **(b)** If $p = 0$, the stability is neutral as in (7.2). However, the diffusion flattens the concentration profile. **(c)** If $p < 0$, the uniform state is stable.

S8. Supplementary data

Replicates of experimental data of Fig. 2b, 2c, 3b, 3c, and 4a. are shown in Fig. S13. The experimental conditions are slightly different. However, this does not affect the conclusions of this paper.

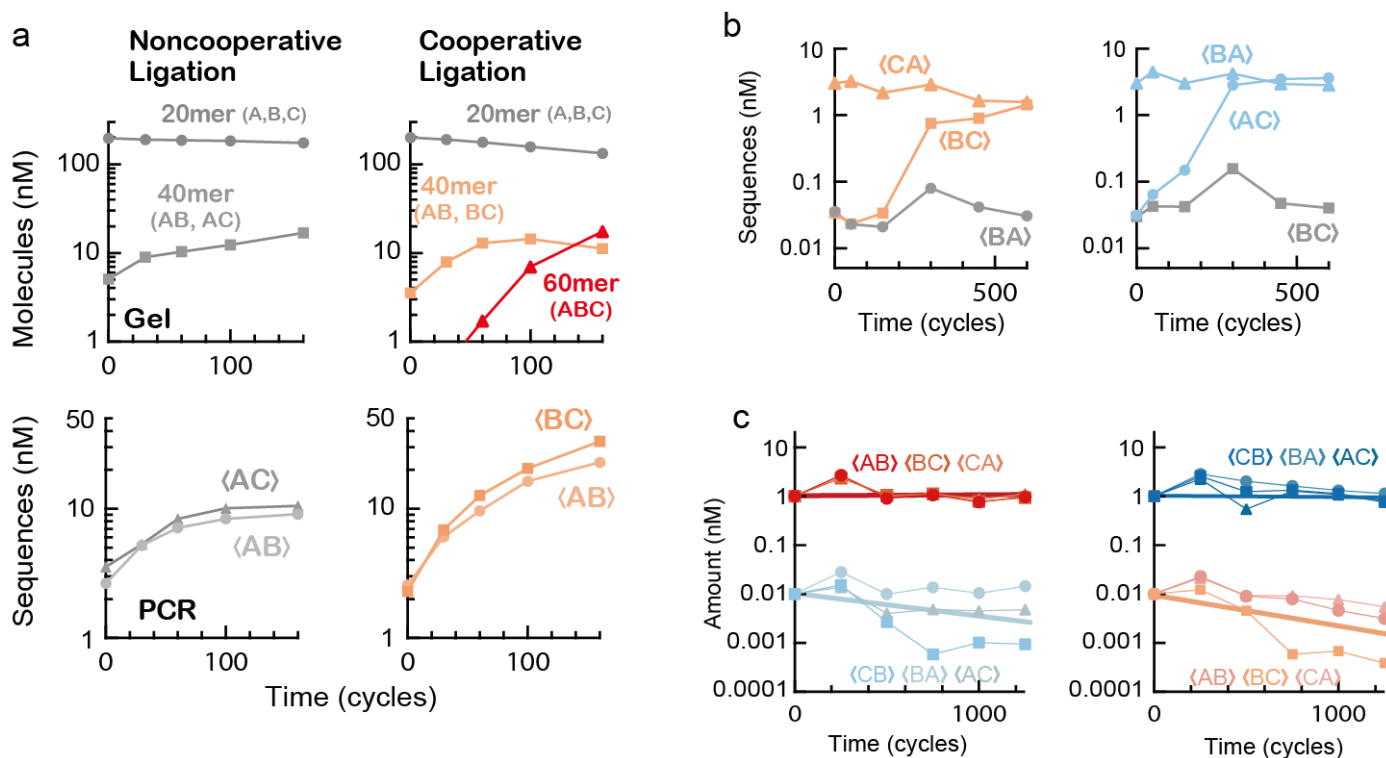


Fig. S13. Replicate experiments for Fig. 2b, c, 3b, c, and 4a. (a) Replicate of Fig. 2b and c, but the initial concentrations of the templates are 2 nM. (b) Replicate of Fig. 3b and c, but the initial concentrations are 2 nM for CA (Left) and BA (Right) and 0.02 nM for BC and BA (Left) and AC and BC (Right). (c) Replicate of Fig. 4a, but the initial concentrations of the templates are 1 nM for the major sequences and 0.01 nM for minor sequences. The dilution rate is 0.47/s. Thick lines are for eye guide.

References

- S1. Barany F, Genetic disease detection and DNA amplification using cloned thermostable ligase, Proc. Nat. Acad. Sci. USA 88, 189-93 (1991)
- S2. Luo J, Barany F, Identification of essential residues in *Thermus thermophilus* DNA ligase, Nuc. Acids Res. 24, 3079-3085 (1996)
- S3. Li J, Wang L, Mamon H, Kulke MH, Berbeco R, Makrigiorgos GM, Replacing PCR with COLD-PCR enriches variant DNA sequences and redefines the sensitivity of genetic testing, Nat. Med. 14, 579-84 (2008)
- S4. Shain EB, Clemens JM, A new method for robust quantitative and qualitative analysis of real-time PCR, Nuc. Acids Res 36, e91 (2008)
- S5. Sambrook J, Russell DW, Molecular Cloning: A Laboratory Manual, CSHL Press (2001)